Theoretical aspects of electrochemistry at low temperature

Isidoro López, Nicolas Le Poul

Version of Record: https://www.sciencedirect.com/science/article/pii/S1572665721001867
Manuscript_f4d413926fe6e420bd8968ef7e465efb

Theoretical aspects of electrochemistry at low temperature

Isidoro López,*[,‡] and Nicolas Le Poul*[,‡]

[‡]Laboratoire de Chimie, Electrochimie Moléculaires et Chimie Analytique, UMR CNRS 6521, Université de Bretagne Occidentale, 6 avenue Le Gorgeu, CS93837, 29238 Brest, Cedex 3, France.

Abstract

This paper aims at providing theoretical basis on electrochemical processes performed at low temperature (*T*) according to three different aspects. First, the effect of *T*-decrease is treated in terms of thermodynamics, mass-transfer, and kinetics of electron transfer (ET) heterogeneous reactions. In particular, predictions of ET kinetics at low temperature are discussed in the frame of Marcus-Hush's model. The second part is focused on the changes associated to temperature decrease for different electrochemical methods including cyclic voltammetry (CV), chronoamperometry (CA), AC Impedance (ACI) and AC voltammetry (ACV). This section gives keys to extract electrochemical data from low-*T* experimental curves. In the third part, theoretical aspects of low-*T* cyclic voltammetry for multiple or chemically-coupled electron-transfer reactions are discussed. CVs of typical molecular mechanisms (EE, EC, ECE…) are provided in order to better visualize the impact of temperature on the redox behavior.

***Keywords**: Low temperature, Cryo-electrochemistry, Electron-transfer kinetics, Chemically-coupled heterogeneous reactions, Molecular electrochemistry.*

1. Introduction

Performing electrochemical and spectroelectrochemical measurements at low temperature (*T*) in liquid and solid electrolytes has always captivated chemists. One main reason for such emphasis is that low temperature offers the possibility to trap and characterize redox species which are not stable at room temperature [1], hence giving insights into mechanistic pathways. Another source of motivation is that quantification of thermodynamics/ kinetics of electron transfer (ET) processes and their chemical-coupled reactions becomes accessible by variation of the temperature. Very first low-*T* electrochemical and spectroelectrochemical works were reported about 50 years ago [2-7], as emphasized by the seminal works of Van Duyne and co-workers [8]. Since, various electrochemical and spectroelectrochemical systems have been designed. These setups have allowed remarkable results in electrochemistry, such as solution-phase voltammetry at temperatures close to liquid nitrogen solidification [9], or studies of electron-transfer kinetics at high-temperature oxocuprate superconductors – liquid electrolyte interfaces [10-15]. UV-Vis-NIR, EPR, Raman and IR spectroelectrochemistry were also developed for low-temperature conditions. For example, time-resolved and *in-situ* UV-Vis cryo-spectroelectrochemistry was recently used to quantify electron transfer kinetics of reactions involving highly unstable copper-peroxide

and superoxide complexes [1]. Alternatively, IR *in-situ* cryo-spectroelectrochemistry was reported for the detection of various transient and unstable organometallic compounds generated by electrochemistry, allowing the rationalization of possible mechanistic pathways [16, 17]. All these significant works, among others, have conducted to the emergence of sophisticated setups based on specific cell designs (depending on the purpose of the experiment), adequate electrolytes (solvent, supporting salt) and electrodes.

Besides, low-*T* electrochemistry and spectroelectrochemistry studies have led to significant advancement in the development and enhancement of theoretical models of electron transfer for heterogeneous processes. Indeed, investigation of ET reactions with standard compounds, such as ferrocene or its derivatives, has allowed the determination of electrochemical parameters (kinetics / thermodynamics / mass transfer) which could be further re-used for comparative analysis. One typical example is the study of electron transfer kinetics at ferrocene-monoalkanethiol self-assembled monolayers at temperatures down to 150 K, which demonstrated the limits of the Butler-Volmer model compared to Marcus-Hush theory [18]. In another example, analytical aspects of chemically-coupled electron transfer reaction were treated and compared to experimental data [19].

Nevertheless, despite much progress has been obtained for nearly 50 years, examples of low-*T* electrochemistry remain scarce essentially because many experimental issues can arise when the temperature is decreased, such as solvent freezing, electrolyte precipitation or water condensation. Moreover, the electrochemical signal is often distorted because of the increased solution resistance ("ohmic drop"). In complement, theoretical treatment of experimental data is not always trivial, notably in terms of kinetics since all processes are slowed down including chemical-coupled reactions. For these reasons, low-*T* electrochemistry and spectroelectrochemistry remain still unattractive to most of chemists and electrochemists.

From this statement, it seems of interest to demystify the theoretical aspects of low-temperature electrochemistry, and make it more accessible to (electro)chemists who wish to use it for the reasons explained above. We thus present here a comprehensive paper on the theoretical aspects of low-*T* electron-transfer electrochemical processes illustrated with simple and typical cases. The aim of the study is to provide theoretical basics in complement to a previous review in which we described the experimental aspects of cryo-electrochemistry and spectroelectrochemistry (cells, solvents, electrolyte, setups) [20]. For this purpose, the present paper is divided into three sections. The first part is focused on the effect of lowering temperature on the thermodynamics, mass-transfer, and kinetics of electron transfer heterogeneous reactions. This section includes a discussion on theoretical models of electron-transfer and a detailed method to predict and calculate kinetic parameters. In the second section, we discuss on the effect of decreasing temperature on the electrochemical signature, according to different electrochemical methods: cyclic voltammetry (CV), chronoamperometry and chronocoulometry (CA, CC), AC Impedance (ACI) and AC voltammetry (ACV). We also provide in this section the type of information which can be extracted from the experimental curves. For each electrochemical method, typical features are briefly recapped such that the discussion can be surveyed by non-specialist readers. The third section is devoted to the theoretical aspects of low-*T* electrochemistry for multiple or chemically-coupled electron-transfer reactions. Since these processes can become easily complicated, CVs of typical cases are given to make it more visually accessible. The paper is completed by concluding remarks and gives future perspectives which can be envisaged.

2. Effect of low temperature on ET thermodynamics, kinetics and mass-transfer

2.1. Thermodynamics of low-*T* electrochemical processes

The standard potential of a redox couple, E^0 (in V) for a monoelectronic heterogeneous electron transfer (Ox + e^- = Red) is classically expressed through the standard free energy of the ET reaction, ΔG^0 (in eV) and the Faraday constant F according to equation (1):

$$\boldsymbol{\Delta G^0 = -FE^0} \quad (1)$$

By default, ΔG^0 and E^0 are defined as the values of the free energy and potential in standard conditions (P = 1 bar), and equal zero for the H^+/H_2 reaction hence defining a referential system. The formal potential $E^{0\prime}$ of a redox reaction is a classical parameter used for reporting experimental data, instead of E^0. It is an adjusted form of E^0 which includes activity coefficients of the Ox and Red forms, γ, as shown in the equation (2):

$$E^{0\prime} = E^0 + \frac{RT}{F} ln \frac{\gamma_{Ox}}{\gamma_{Red}} \quad (2)$$

The equation (2) indicates that the variation of the formal potential $E^{0\prime}$ for a redox reaction with temperature can be due to two effects. A first possible source of variation springs from the RT/F factor which impacts the ratio of the activity coefficients $\gamma_{ox}/\ \gamma_{red}$. If this latter ratio is superior to 1 and considered as temperature-independent, the decrease in T induces a negative shift of the formal potential. This situation would occur if the variation of the electrostatic charge upon electron transfer is not well compensated by the electrolyte. The second source of variation of $E^{0\prime}$ with T is correlated to the standard potential itself. According to the equation (3), the standard free energy $\Delta G^0$of a redox reaction includes an enthalpic term, ΔH^0 (in eV) as well as a temperature-dependent entropic term, $T\Delta S^0$ (where ΔS^0 is expressed in eV/K).

$$\Delta G^0 = \Delta H^0 - T\Delta S^0 \quad (3)$$

The standard entropy ΔS^0 can be expressed from the dependence of ΔG^0 with T, according to equation (4):

$$\Delta S^0 = -\left(\frac{\partial \Delta G^0}{\partial T}\right)_P = nF\left(\frac{\partial E^{0\prime}}{\partial T}\right)_P \quad (4)$$

It appears from this equation that a positive shift of the formal potential upon T decreasing can be inferred to an entropic gain. Such situation was reported for example by Savéant and co-workers with a series of basket-handle iron porphyrins [21]. These authors calculated the standard reaction entropy ΔS^0 (normalized by the Faraday constant) from the slope of $E^{0\prime}$ *vs.* T plots. They interpreted this effect to the ordering of the basket-handle

structure triggered by the increased interaction of solvent molecules with the negative charges upon electron transfer.

A further step consists in taking into account the temperature-dependency of ΔH^0 and ΔS^0 as given in equations (5-8) :

$$\left(\frac{\partial \overline{H}^0}{\partial T}\right)_P = \bar{C}_P{}^0 \qquad (5)$$

$$\left(\frac{\partial \Delta\overline{H}^0}{\partial T}\right)_P = \Delta\bar{C}_P{}^0 \qquad (6)$$

Although the heat capacity at constant pressure, $\bar{C}_P{}^0$, is by no means negligible, the reaction increment $\Delta\bar{C}_P{}^0$ is often very small for experiments within a range of ΔT = 100 K [22]. This is particularly true for gas phase reactions which do not involve much change in freedom of molecular motion. For liquid-phase reactions, $\Delta\bar{C}_P{}^0$ values concern processes that entail the creation or neutralization of electrical charges. Thus, the $\Delta\bar{C}_P{}^0$ value is essentially correlated to the solvation of ions. Indeed, a major change in solvation may modify the freedom of motion of molecules. This has an effect on $\Delta\bar{C}_P{}^0$ which can be large compared to the heat capacity change that would be associated with the reaction in the absence of solvent, especially if the reaction involves changes in only one or two bonds.

Just as in the case of the enthalpy, the variation of $\Delta\overline{S}^0$ with T is seldom observed. Formally the variation of the entropy is given by equations (7) and (8):

$$\left(\frac{\partial \overline{S}^0}{\partial T}\right)_P = \frac{\bar{C}_P{}^0}{T} \qquad (7)$$

$$\left(\frac{\partial \Delta\overline{S}^0}{\partial T}\right)_P = \frac{\Delta\bar{C}_P{}^0}{T} \qquad (8)$$

From equations (7) and (8), the variation of entropy with temperature, over a narrow temperature range, is proportional to that of the enthalpy, and the slope of the relationship is equal to the average value of 1/*T.* This is the reason for the cancellation of errors in simultaneously neglecting the variation of both enthalpy and entropy with temperature in computing the free energy according to equation (3) [23].

2.2. Mass-transfer of low-*T* electrochemical processes

Mass transfer of a species "*j*" in solution occurs by diffusion, migration, and convection. Diffusion and migration result from a gradient in electrochemical potential, $\bar{\mu}_j$, whereas convection results from an imbalance of forces on the solution. For linear mass transfer, the classical Nernst-Planck equation [24] is simplified into

equation (9) where J_j, D_j, C_j, and z_j are the flux, diffusion coefficient, concentration and charge of the species *j*, respectively:

$$\boldsymbol{J_j(x) = -D_j \frac{\partial C_j}{\partial x} - \frac{z_j F}{RT} D_j C_j \frac{\partial \phi}{\partial x} + C_j v(x)} \qquad (9)$$

The migration term of the equation (9) is usually neglected by working with low concentration in electroactive species compared to that of the supporting electrolyte (100 times less) [25]. In addition, the convection term of the equation (9) cancels when short-time electrochemical methods such as cyclic voltammetry or chronoamperometry are carried out in quiescent solutions. In consequence, the current response becomes a balance between the rate of electron transfer from or to the electrode and the diffusion of the electroactive species. The Stokes-Einstein law correlates the diffusion coefficient *D* of a spherical species of radius *r* with *T* and the temperature-dependent solvent dynamic viscosity η_s as shown in equation (10):

$$\boldsymbol{D = \frac{k_B T}{6\pi r \eta_s}} \qquad (10)$$

Accordingly, a decrease of the temperature affects the diffusion coefficient through both *T* and η_s terms of equation (10), considering *r* as constant. The variation of dynamic viscosities with *T* for pure liquids and mixtures of solvents was shown to follow an Arrhenius-type deviation [22]. For instance, η_s increases by almost 2-fold (0.46 to 0.85 mPa s) for tetrahydrofuran when *T* drops from 298 K to 248 K [22]. Hence, the diffusion coefficient *D* in equation (10) varies in an exponential manner $vs.\ T^{-1}$, as a thermally-activated process. Since the flux is proportional to *D* in a diffusion-controlled regime, the resulting current density at the electrode surface displays an Arrhenius-like behavior. Such condition is of interest for the determination of the activation enthalpy for diffusion $\Delta H^{\neq}$ by plots of $ln(D)\ vs.\ T^{-1}$.

In a more general manner, electrochemical measurements at low temperature dramatically affect all mass transfer contributions including migration and convection. Migration effects for the electroactive species are usually cancelled at room temperature by the presence of large excess of non-electroactive supporting electrolyte. In addition, the ohmic drop, which is the resistance R_{unc} to the pass of current into the solution between the working and the reference electrode, is minimized. At low temperatures, the increase of the viscosity of the solution impacts the net resistance of the solution: the mobility of the supporting electrolyte ions decreases linearly with the viscosity of the medium according to the Stokes law. Thus the applied potential can strongly differ from the real potential in the working electrode due to the ohmic drop.

The increase of the ohmic drop observed at low temperature is usually balanced with an increase of the concentration of supporting electrolyte, such that the net conductivity of the solution remains acceptable. However, measurements at very low temperatures can eventually produce the precipitation of the supporting electrolyte. Additionally, the decrease of the concentration of electrolyte due to precipitation and subsequently the ratio between supporting electrolyte and electroactive species concentrations induces the incapacity of the system (mainly constituted by the supporting electrolyte in terms of concentration) to disperse electrical fields formed in the interface between the working electrode and the diffusion layer zone [25] generating a gradient of

potential and so letting the migration term in equation (9) to contribute to the mass transfer. Under these circumstances the mathematical treatment of the system becomes more complex and the Poisson equation must be invoked [25].

2.3. Kinetics of low-T electrochemical processes

Most of condensed-phase reactions are characterized by a temperature-dependent standard rate constant k^0, according to an Arrhenius expression that includes a pre-exponential frequency factor A' and a standard free energy of activation $\Delta G_0^{\neq}$ (equation (11)):

$$k^0 = A' \exp\left(-\frac{F\Delta G_0^{\neq}}{RT}\right) \qquad (11)$$

Where the pre-exponential factor A' includes a dimensionless entropic term $\Delta S^{\neq}/R$.

According to these simple considerations, the kinetics of electron transfer reactions and associated chemical processes are expected to decrease with temperature according to an Arrhenius behavior, i.e. the standard rate constant k^0 decreases exponentially with T^{-1}. Another interesting information to earn from equation (11) is that the temperature variation of k^0 can be predicted from calculated values of the standard free energy of activation $\Delta G_0^{\neq}$ and the pre-exponential factor A'. For that purpose, it is possible to rely on ΔG^0.

The popular Butler–Volmer (BV) model proposes that the variation of the driving force induces a linear deviation of both according to the value of the transfer coefficient α (see Appendix A for details). [26]. In spite of its relative simplicity and practical usefulness, the empirical Butler-Volmer approach does not allow predicting and calculating the free enthalpies of activation because molecular structures of the reactants and solvent are not taken into account. Moreover, when the ET reaction necessitates high driving force (such as at ultra-low temperatures), the Butler-Volmer model is no longer appropriate since it assumes that the free energy is much smaller than the reorganizational energy barrier (see discussion below on Marcus-DOS model) [27].

A more sophisticated strategy is based on the Marcus-Hush model, which gives the possibility to consider the properties of the medium (solvent, supporting electrolyte), the electrode and the electroactive species in the calculations [24, 28]. In their model, Marcus and co-workers assumed, from statistical calculations, a quantum mechanical splitting at the intersection between the reactant and product free energy surfaces that, while large enough to ensure adiabaticity, was not large enough to significantly affect the activation free energy [29, 30]. The resulting expressions for the Gibbs energies of activation associated with the forward and backward reactions for an heterogeneous electron transfer, $\Delta G_{\mathrm{f}}^{\neq}$, $\Delta G_{\mathrm{b}}^{\neq}$, are given in equations (12) and (13):

$$\boldsymbol{\Delta G_{\mathrm{f}}^{\ddagger}} = \frac{\boldsymbol{\lambda}}{\mathbf{4}}\left(\mathbf{1} + \frac{\boldsymbol{F(E-E^0)}}{\boldsymbol{\lambda}}\right)^{\mathbf{2}} \qquad (12)$$

$$\Delta G_b^{\ddagger} = \frac{\lambda}{4}\left(1 - \frac{F\left(E - E^0\right)}{\lambda}\right)^2 \qquad (13)$$

where λ is the reorganization energy, which represents the energy necessary to transform the nuclear configurations in the reactant and the solvent to those of the product state.

The two equations (12) and (13) indicate that forward and backward free activation energies, thus rate constants, can be calculated knowing λ, which itself varies with solvent, supporting electrolyte, electrode and electroactive species properties. Hence, the temperature dependence of electron transfer kinetics appears as predictable from the theoretical determination of λ. An Arrhenius-like expression of the standard rate constant k^0 corrected from solvent dynamics can be obtained by several numerical treatments and approximations (see Appendix B for details), as given in equation (14) [31]:

$$\boldsymbol{k^0} = \boldsymbol{\kappa}_{el}\boldsymbol{K}_P\left(\frac{\boldsymbol{3Da}}{\boldsymbol{8r^3}}\right)\left(\frac{\boldsymbol{\varepsilon}_s}{\boldsymbol{\varepsilon}_\infty}\right)\left(\frac{\boldsymbol{\lambda}_o}{\boldsymbol{\pi R}}\right)^{\boldsymbol{1/2}}\left(\frac{\boldsymbol{1}}{\boldsymbol{T}}\right)^{\boldsymbol{1/2}}\exp\left[-\frac{\boldsymbol{\lambda}}{\boldsymbol{4RT}}\right] \qquad (14)$$

Where the outer-sphere reorganization energy λ_o, is expressed as in equation (15) by considering the solvent as a dielectric continuum:

$$\boldsymbol{\lambda}_o = \frac{\boldsymbol{N_A e_0^2}}{\boldsymbol{8\pi\varepsilon_0}}\left(\frac{\boldsymbol{1}}{\boldsymbol{a}} - \frac{\boldsymbol{1}}{\boldsymbol{R}}\right)\left(\frac{\boldsymbol{1}}{\boldsymbol{\varepsilon}_{op}} - \frac{\boldsymbol{1}}{\boldsymbol{\varepsilon}_s}\right) \qquad (15)$$

[In these two equations, κ_{el} is the electronic transmission coefficient (related to the probability of electron tunneling), K_P is a precursor equilibrium constant representing the ratio of the reactant concentration in the reactive position at the electrode (the precursor state) to the concentration in bulk solution, D and a are, respectively, the diffusion coefficient and hydrodynamic radius of the electroactive species and r the radius of the solvent molecule, ε_s and ε_∞ are the static (zero frequency) and high-frequency dielectric constants respectively, N_A is the Avogadro constant, e_0 is the fundamental electronic charge, ε_{op} is the optical dielectric constant, ε_0 is the permittivity of free space, and R is taken as the distance from the center of the molecule to the electrode].

The equation (14) can thus predict how the standard rate constant for a known reaction with known parameters (diffusion coefficients, size of redox species, dielectric constant of the solvent) would vary with temperature, assuming an adiabatic case. It also gives the possibility to determine the outer-sphere reorganizational energy from experimental values of k^0 from linear plots of $\ln\left(k^0 T^{1/2}\right)$ against T^{-1}. Thus, the Marcus model appears as a powerful and tunable approach for theoretical predictions of the variation of ET kinetics with temperature.

However, since Marcus theory is only concerned with energy states at the Fermi level, an extensive theory for heterogeneous electron transfer, accounting for the electronic structure of the electrode, *via* the density of states parameter, has been proposed [32, 33]. This theory, called the Marcus-density of states (Marcus-DOS) theory, has been used mainly for simulation of cyclic voltammetry data [14, 32-34]. Hence, for an oxidation process,

electron transfer takes place, mostly, from the electronic state of the redox species to the states near the Fermi level of the electrode. However, this assumption is no longer valid case when, for example, the applied potential E is such that $|(E - E^0)|$ is large (as it can occur at low temperature due to slow ET kinetics). In this situation, all electronic states with which electron can be exchanged have to be considered and not only those related to transfers to states near the Fermi level as it is the case with Marcus theory. An electron transfer for an oxidation process occurs if an empty state of energy ε in respect to the Fermi level ε_F , is available on the electrode surface. The probability of finding such an empty state is $\rho(\varepsilon)\big(1 - f(\varepsilon)\big)$, where $\rho(\varepsilon)$ is the density of electronic states on the metal surface and $f(\varepsilon)$ is the Fermi-Dirac distribution :

$$\boldsymbol{f(\varepsilon)} = \frac{\mathbf{1}}{\mathbf{1}+\exp\left[\frac{\varepsilon-\varepsilon_F}{k_B T}\right]} \tag{16}$$

The forward and backward rate constants for this electron transfer are then expressed according to equations (17) and (18) (see Appendix C for expressions of free energies of activation):

$$\boldsymbol{k_f(\varepsilon)} = [(\mathbf{4\pi\lambda k_B T})]^{-1/2} \boldsymbol{A' \int \rho(\varepsilon) f(\varepsilon) \exp\left[-\frac{[\lambda-\varepsilon+F(E-E^0)]^2}{4\lambda k_B T}\right] d\varepsilon} \tag{17}$$

$$\boldsymbol{k_b(\varepsilon)} = [(\mathbf{4\pi\lambda k_B T})]^{-1/2} \boldsymbol{A' \int \rho(\varepsilon)[1 - f(\varepsilon)] \exp\left[-\frac{[\lambda+\varepsilon-F(E-E^0)]^2}{4\lambda k_B T}\right] d\varepsilon} \tag{18}$$

where A' is the pre-exponential factor.

In all these formulae, it is assumed that the same reorganization energy λ applies to both the forward and backward reactions. Several approximations can be made to simplify the calculations. The first one is to assume that the density of states near the Fermi level varies so slowly that it can be considered as constant. Moreover, equations (17) and (18) can be largely simplified depending on the value of $|(E - E^0)|$ compared to λ. When $E \cong E^0$, only the region near the Fermi level contributes to the total current, and the current densities get similar to those observed considering Butler-Volmer approach for kinetics. When the value of $|(E - E^0)|$ is large, one obtains a limiting current which is independent of the applied potential. Interestingly, the inverted region predicted by the Marcus-Hush theory disappears when all electrode electronic states are taken into account in Marcus-DOS model. This is a consequence of the electronic states below the Fermi level which are thermodynamically unfavorable but kinetically advantageous. Overall, the effects of the temperature decrease on the electron transfer kinetics by using the Marcus-DOS are similar to those described for the Marcus-Hush model. However, the Marcus-DOS gives the opportunity to take into account the physical properties of the electrode material, which is of particular interest when considering non-metal electrodes, such as semi-conductors and superconductors, whose conduction properties are fully temperature-dependent. Finally, the effect of asymmetry in λ on the electron transfer kinetics of forward and backward processes has been recently addressed by Compton and co-workers [35]. This asymmetry appears as a consequence of significant differences between the vibrational modes of the oxidized and reduced species.

From a more general viewpoint, it appears that different kinetic models can be used for the analysis of low-temperature experimental data. For instance, it was shown that electron-transfer kinetics of simple ET reactions could be estimated from the Butler-Volmer model, by considering only the variation of the peak-to-peak separation (ΔE_p) with scan rate v from CVs and not the waveshape of the voltammograms [27]. This approach is the same as used for sluggish processes at room temperature as proposed by Laviron [36], or Nicholson and Shain [37]. It is based on the assumption that the driving force $|F(E-E^0)|$ is significantly smaller than the reorganizational energy λ, thus works well with redox systems with high value of λ (high dipolar reorientation energies of the solvent and electrolyte). Nevertheless, as previously stated, when the $|F(E-E^0)| \,/\, \lambda$ ratio is not small, the Butler-Volmer is no longer valid and the Marcus' model better mimics the experimental behaviour [27]. To better visualise this discrepancy, we have simulated CVs (Figure 1) for a simple electron transfer reaction which approaches low-temperature conditions according to previously reported experimental data (k^0 = 10^{-5} cm s^{-1}, D = 10^{-7} cm^2 s^{-1}) [31]. CVs have been computer-generated by considering the Marcus-DOS model for different values of λ (from 0.1 to 1 eV), and the Butler-Volmer approximation for α = 0.5. The resulting graph in Figure 1 displays how the value of the reorganization λ can deeply impact the peak shape and peak currents, whereas the peak potential undergoes slight variation. In particular, the situation for which λ has the smallest value (0.1 eV) features a significant decrease of peak current intensities as well as a broadening of the waves, compared to the Butler-Volmer case. The large broadening of the peaks can be interpreted as the occurrence of a kinetic regime where ET rates become ultimately independent of free energy [27]. Finally, it appears that adequate analysis of low-T experimental CVs by the Marcus-DOS approximation allows the accurate determination of the reorganizational energy in contrast to the Butler-Volmer model, as previously reported for ferrocene derivatives [18, 27, 34, 38].

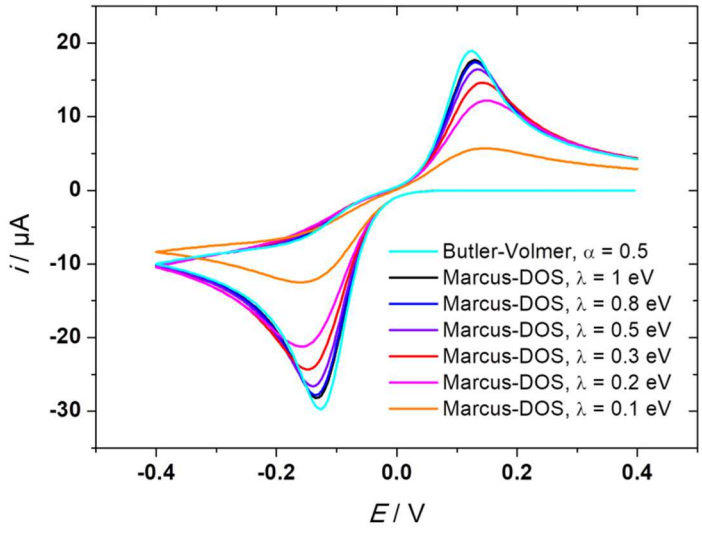

Figure 1. Simulated CVs for a simple monoelectronic electron transfer ($\boldsymbol{C}$ = 1 mM, $\boldsymbol{A}$ = 1 cm^2, $\boldsymbol{v}$ = 0.1 V/s) assuming a Marcus-DOS model for different values of $\boldsymbol{\lambda}$ (from 0.1 to 1 eV), and the Butler-Volmer approximation with $\boldsymbol{\alpha}$ = 0.5. To account for low-T conditions, the standard rate constant was taken as $\boldsymbol{k^0}$ = 10^{-5} cm s^{-1} and the diffusion coefficients as $\boldsymbol{D}$ = 10^{-7} cm^2 s^{-1}. Simulations performed by using the Digielch© software.

2.4. Double layer effects

The popular Gouy-Chapman-Stern (GCS) model of the electrode-electrolyte interface assumes that solvated ions cannot approach at a closer distance x_2 from the electrode than that defined as the Outer Helmholtz Plane (OHP), the potential at the OHP being ϕ_2 [24]. On one hand, the compact layer between the electrode and the OHP ($x < x_2$) contains molecules (solvent, ions) which are specifically adsorbed. On the other hand, the region beyond the OHP (diffuse layer) is constituted of solvated molecules whose concentration varies with the distance to the OHP ($x > x_2$), itself dependent on the potential which is applied to the electrode. Hence, according to the GCS model, the inverse of the differential capacitance C_d results from the sum of the reciprocals compact and diffuse layers capacitances, C_H and C_D, respectively, as shown by equation (19) for a z:z electrolyte:

$$\frac{1}{C_\mathrm{d}} = \frac{1}{C_\mathrm{H}} + \frac{1}{C_\mathrm{D}} = \frac{x_2}{\varepsilon_\mathrm{s}\varepsilon_0} + \frac{1}{\left(2\varepsilon_\mathrm{s}\varepsilon_0 z^2 e^2 n^0/k_B T\right)^{1/2}\cosh\left(ze\phi_2/2k_B T\right)} \qquad (19)$$

Where x_2 is the distance of the OHP from the electrode, ε_0 the permittivity of free space, ε_s the static dielectric constant, z the charge of the solvated ion at the OHP, e the charge on the electron, n^0 the bulk concentration, k_B the Boltzmann constant, T the temperature and ϕ_2 the potential at the OHP.

Thus, the GCS model predicts that C_D becomes predominant over C_H at low electrolyte concentration and low polarization, implying that C_D varies in a V-shaped fashion with the potential under these conditions. Inversely, at high electrolyte concentration and/or high polarization, C_d approximates C_H and is potential independent.

The potential drop within the compact layer accounted by the GCS model also impacts the kinetics of the electron transfer. One reason is that the concentration of electroactive species at the OHP differs from that in the bulk solution. Another cause is that the driving force of the electrochemical reaction, that is the free energy of the process, can vary according to the values and signs of the charge z and the potential ϕ_2 at the OHP (which is slightly different from the bulk one).. Consequently, the forward and backward activation free energies of the Butler–Volmer approximation may be recalculated so as to obtain for the "true" standard rate constant, k_t^0, called as the Frumkin correction. For the forward reaction the following expression can be derived [24]:

$$k_\mathrm{t}^0 = k^0 \exp\left[\frac{-(\alpha - z)F\phi_2}{RT}\right] \qquad (20)$$

where k^0 is the standard kinetic constant in the absence of Frumkin effects and z is the electric charge of the eletroactive species.

From these equations, it is expected that decreasing of the temperature may have some effect on the value of the double layer capacitance. In the case of high electrolyte concentration / high polarization, the compact layer can be considered as in the Helmholtz model, i.e. as a simple two-plate capacitor for which $C_\mathrm{d} = C_\mathrm{H}$. In that particular case, the differential capacitance varies with ε_s supposing x_2 as constant from the first term of equation (19). Literature data indicate that ε_s increases when T decreases for electrochemical solvents such as water, acetonitrile, THF. For example, a temperature decrease from 298 K to 175 K in THF induces a two-fold

increase of ε_s and consequently C_d from equation (19) [31]. The situation becomes more complicated at lower concentration in electrolyte and low polarization because the diffuse layer term, C_D, of equation (19) becomes non negligible. The temperature-dependence of the capacitance is then a function of ε_s, T and the potential at the OHP ϕ_2. In terms of kinetics of electron transfer, k_t^0 can diverge significantly from k^0 and the difference is exacerbated at low temperature. Considering a typical reduction process found in coordination chemistry where α =0.5, z =+2 and ϕ_2 = -50 mV, the ratio k_t^0/k^0 is 0.05 at 298 K and 0.007 at 175 K, hence significantly varying with temperature.

3. Electrochemical methods at low temperatures

In the previous section, we have discussed about the effect of temperature in terms of thermodynamics, mass-transfer and kinetics of simple electron transfer reactions. We have shown that Marcus-Hush and Marcus-DOS theoretical models could also predict the temperature variation of electron transfer dynamics for a given reaction (solvent, electroactive species, electrode…). In the following section, we aim at providing the main effect of temperature on the electrochemical signature and the type of information which can be extracted from the experimental curves. Amongst the many electrochemical techniques which have been developed, we have chosen to focus on the most well-known methods: cyclic voltammetry (CV), chronoamperometry and chronocoulometry (CA, CC), AC Impedance (ACI), and AC voltammetry (ACV). This list is not exhaustive and several other methods can also be used for low-temperature studies [24]. In order to better explain the effect of temperature, we have made the choice to briefly recap the typical features of each technique such that the discussion could be followed by non-specialist readers.

3.1. Cyclic voltammetry

Cyclic voltammetry is probably the most used and well-known electrochemical technique since many important data can be obtained from the experimental curves. The technique consists in measuring the current produced at the working electrode during the linear sweep of the potential (*vs.* a fixed reference electrode) according to a cycle (forward and backward scans). The most significant advantage of CV is the simple variation of the sweep rate (scan rate) which allows changing the time window of the measurements, giving access to the kinetics.

Room temperature voltammetry for a reversible monoelectronic electron transfer involving free-diffusing electroactive species is given in Figure 2-A. The peak-to-peak separation $\Delta E_p = E_{pa} - E_{pc}$ equals 2.22 RT/F, hence approximatively 57 mV at 298 K, where E_{pa} and E_{pc} are defined here as the anodic and cathodic peak potentials. On the other hand, the anodic and cathodic peak currents i_{pa} and i_{pc} are expressed through the Randles-Ševčik equation (21) (assuming n=1) [24]:

$$\boldsymbol{i_p = 0.446\left(\frac{F^3}{RT}\right)^{1/2} AD^{1/2}Cv^{1/2}} \qquad (21)$$

Where A is the electrode area, D and C are the diffusion coefficient and concentration in electroactive species, respectively.

On this simple basis, the value of ΔE_p on the CV would theoretically decrease by several millivolts with temperature (it would drop from 57 mV at 298 K to 33 mV at 175 K, for example). Moreover, the peak current would slightly increase when T diminishes (approximatively 25% over 100 K variation), assuming D as constant. Of course, these simple predictions are opposite to what is observed in reality because temperature-dependent factors including mass transfer (controlled by the scan rate), electron transfer kinetics, solution resistance and double layer capacitance have to be taken into account. Charge transfer kinetics is the main parameter affecting ΔE_p. As shown through the Arrhenius-like equation (11), the standard rate constant k^0 decreases exponentially with $-1/T$ according to the standard free energy of activation $\Delta G_0^{\neq}$ and the pre-exponential factor A'. One consequence of the sluggishness of the electron transfer reaction is the modification of the voltammetric curve, the system becoming irreversible. Under these conditions, the expression of the potential deviates from the Nernst equation since the electron transfer is no longer under thermodynamic control. The peak potential can then be expressed as in equation (22) [24]:

$$\boldsymbol{E_p = E^{0\prime} - \frac{RT}{\alpha F}\left[0.78 + ln\left(\frac{D^{1/2}}{k^0}\right) + ln\left(\frac{\alpha F v}{RT}\right)^{1/2}\right]} \qquad (22)$$

As previously mentioned, the diffusion coefficient value D decreases with temperature because diffusion is a thermally activated process. Hence, the relative shift of E_p *vs.* $E^{0\prime}$ in equation (22) is highly dependent on the $(D^{1/2}/k^0)$ ratio. As the temperature is decreased, this ratio mainly increases because of the large energy of activation (inner and outer-sphere) required at the electrode surface to accommodate the electron transfer. By comparison, the effect of diffusion remains modest. The effect of T on ΔE_p is exacerbated by the ohmic drop and, in a less significant manner, by double layer effects (see section 2). Increase of the solution resistance (also coined uncompensated resistance), R_{unc}, typically from tens of Ω at room temperature to several thousands of Ω at low T induces a shift of the peaks towards more negative values for a reduction process and more positive for an oxidation reaction. In highly resistive media as encountered at very low temperature, these shifts can attain several hundreds of mV. Once effects due to ohmic drop have been considered, the variation of ΔE_p with temperature can be determined to analyze the evolution of the heterogeneous electron-transfer rate constant with a decrease in temperature. For instance, Diao and Zhang exploited this approach to compare the value of the heterogeneous constant at different temperatures for the five quasireversible one-electron reductions of C_{60} [39]. For all electrochemical processes, an approximately one-order decrease of the rate constant was found when T was decreased from 293 K to 223 K.

The sluggishness of the electron transfer at low temperature also induces a change in the expression of the peak current, which is modulated by the square-root of the symmetry coefficient α [24]:

$$\boldsymbol{i_p = 0.496\left(\frac{F^3}{RT}\right)^{1/2}\alpha^{1/2}AD^{1/2}Cv^{1/2}} \qquad (23)$$

In the most typical case, α = 0.5, which induces that the current is 4 times less when changing from a reversible to an irreversible process (equations (21) and (23)). In addition, when lowering temperature, the loss of current occurs because of the lowering of the diffusion coefficient. Over a 100 K drop, D can typically goes from 10^{-5} cm^2 s^{-1} to 10^{-7} cm^2 s^{-1}, meaning a 10-times decrease of the current peak assuming irreversible cases [31].

The Figure 2 exemplifies well these variations. The CVs have been simulated for a redox couple for a wide range of temperatures (120-300 K) assuming variation of diffusion coefficients and standard rate constants according to the following parameters taken from literature data for the $DMeFc^{+/0}$ couple [27, 31]: $\Delta G_0^{\neq}$ = 22 kJ mol^{-1}; A' = 2 × 10^3 cm s^{-1}; $\Delta H_D^{\neq}$ = 13 kJ mol^{-1}; A'_D = 0.01 cm^2 s^{-1}. The system is fast at room temperature as shown by the low peak-to-peak separation. Between 300 K and 200 K (Figure 2-A), the main effect observed is the progressive decrease of the peak current whereas ΔE_p remains almost constant. This originates purely from the decrease of the diffusion coefficient in a square-root manner. The system remains however reversible because the kinetics of electron transfer are still fast (*vs*. mass transfer) within the timescale of the experiment (v = 0.1 V s^{-1}). Hence, the redox system obeys equation (21). Below 200 K, a supplementary effect occurs: the peak-to-peak separation dramatically increases to reach approximatively 230 mV at 120 K (Figure 2-B). Hence, the electron transfer kinetics is no longer fast and the system passes from the reversible behavior to the quasi-reversible and irreversible ones (from 160 K). It then follows the equations (42) and (43). Note that the same simulations carried out at a higher scan rate (for example v = 1 V s^{-1}) would have led to different response, since the flux of electroactive species would be enhanced. As a consequence, irreversibility measured through the start of increase of ΔE_p would have appeared at higher temperature than 200 K.

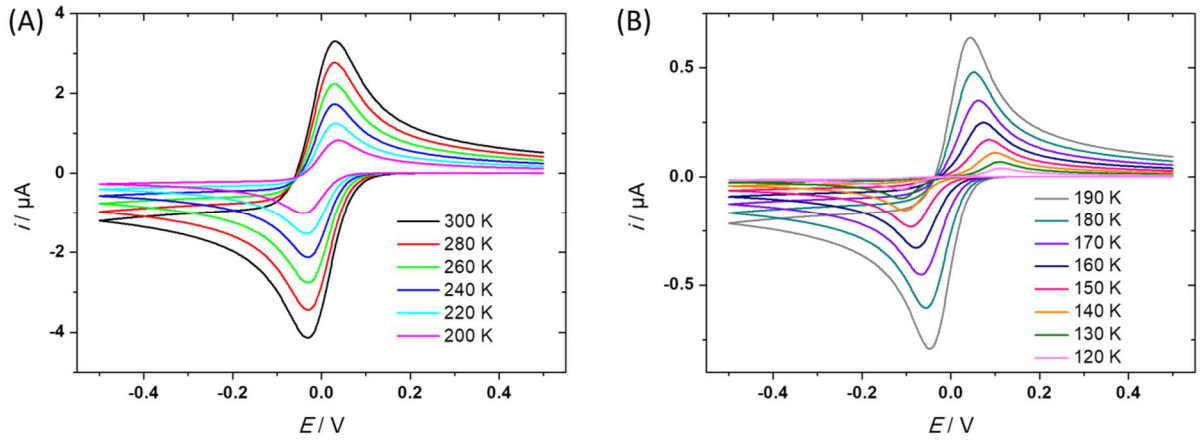

Figure 2. Simulated CVs illustrating the effect of the temperature on the shape of the voltammogram for a mono-electronic process involving a free-diffusing electroactive species. C_{ox} = 1 mM, D_{ox} = D_{red} = 10^{-5} cm^2 s^{-1}, k^0 = 1 cm s^{-1}, A = 0.01 cm^2. Simulations were carried out with the software Kissa-1D [40].

Other aspects have also to be taken into account when performing low-T cyclic voltammetry, and more generally electrochemical techniques. The first one is the value of the potential which is measured against that of the reference electrode. Most of experimental measurements are carried out with a pseudo-reference electrode, such as a Pt or Ag wire directly dipping in the solution. The potential of the redox species is then adjusted by adding a known redox couple in the solution, such as ferrocenium/ferrocene, at the end of the experiment, and then referred to it. This method has the inconvenient to bring other reactive species in the medium, such water and

oxygen, and possibly make them react with electroactive compounds. Another possibility is to use stable and known organic references electrode, such as $Ag/AgNO_3$ or $Ag/AgClO_4$, which can be placed either inside or outside the low-T cell. Indeed, the equilibrium potential of these known reference electrodes follows a Nernst law and then shifts with temperature according to a RT/F factor. Hence, a ΔT = 100 K decrease from room temperature would induce an 8 mV shift. Using a thermostated reference electrode out of the cell is probably the most convenient way to obtain accurate data, if one minimizes the variation of the liquid junction potential with temperature (estimated as 0.01 mV K^{-1}) [8]. Indeed, concentration gradients in the reference electrode salt bridge due to thermal diffusion (the Soret effect) and the resulting changes in the effective reference electrode potential are negligible.

Another parameter of importance for low-temperature cyclic voltammetry is the change in concentration due to volume contraction. The decrease of the volume is related to the increase of the density of the solvent through the cubic expansion coefficient α_{exp} as defined in equation (24) [22]:

$$\boldsymbol{\alpha}_{\text{exp}} = (\mathbf{1}/\boldsymbol{V})(\boldsymbol{\partial V}/\boldsymbol{\partial T})_{\boldsymbol{P}} \qquad (24)$$

The values of α_{exp} are fully solvent-dependent and close to 0.001 C^{-1}. For instance, methylene chloride displays α_{exp} = 0.00126 C^{-1} whereas acetone exhibits α_{exp} = 0.00146 C^{-1} [22]. This indicates that a 100 K decrease in temperature would decrease the volume approximatively by 13% and 15% in these solvents, respectively, hence increasing the concentration by the same amount. However, this effect is likely compensated by the lower solubility of the electroactive species when T decreases. Hence, the real concentration in redox compounds is hard to determine at low temperature except if other methods, such as UV-Vis spectroscopies, can be coupled under the same conditions.

At last, it should be noted that the Randles- Ševčik equation (21) (and indirectly the Cottrell equation (25), see below) applies for electrochemical reactions under semi-infinite linear diffusion regime. For instance, this equation cannot be used for analysis of voltammetric experiments with ultramicroelectrodes, since their low radius r allows radial diffusion, leading to S-shaped CVs. This steady-state regime occurs only when $v << RTD/nFr^2$ [24]. Accordingly for ultramicroelectrodes, decreasing T (thus concomitantly D) induces a decrease of the scan rate value at which the steady-state regime can be kept. In other words, when using microelectrodes for cryovoltammetry, lower scan rates should be used to maintain S-shaped CVs.

3.2. Chronoamperometry and chronocoulometry

Chronoamperometry is a well-known electrochemical technique which consists in measuring the current *vs.* time resulting from a subtle stepping of the potential from an initial value E_i to a final value E_f. On one hand, E_i is usually pre-determined from CV measurements by taking a value for which no current flows ("rest" potential). On the other hand, the final potential E_f corresponds to a potential value for which a redox reaction takes place and is diffusion-controlled. It is usually adjusted to a value ≈ 60 - 100 mV beyond the peak potential on the CV. The classical Cottrell equation gives the expression of the measured current $i_f(t)$ against the time t, as shown in equation (25) for reversible electron transfer [24]:

$$\boldsymbol{i_f(t) = \frac{nFACD^{1/2}}{\pi^{1/2}t^{1/2}}} \qquad (25)$$

Hence, chronoamperometry appears as the method of choice for the determining diffusion coefficient D of the electroactive species knowing its bulk concentration, the area of the electrode A and the number of electrons n involved in the redox process. The equation (45) is still valid when the temperature is lowered as long as E_{fin} is finely adjusted to reach the diffusion-controlled zone. Correction of the concentration, as previously discussed for cyclic voltammetry, due to lower solubility and solvent contraction, may be introduced for a more accurate determination of D. Since diffusion displays an Arrhenius-like behavior, its activation enthalpy $\Delta H_D^{\neq}$ can be obtained from plots of $ln(D)$ *vs.* T^{-1}. The Figure 3 displays simulated chronoamperograms for a wide range of temperature, as performed for cyclic voltammetry. As expected, the measured current decreases with temperature in agreement with the Cottrell equation because of the decrease of the diffusion coefficient. Since the effect of convection decreases with T, the time window for analysis of plots of i *vs.* $t^{-1/2}$ can be slightly enlarged at low temperatures. However, no kinetic data about electron transfer can be obtained from these curves.

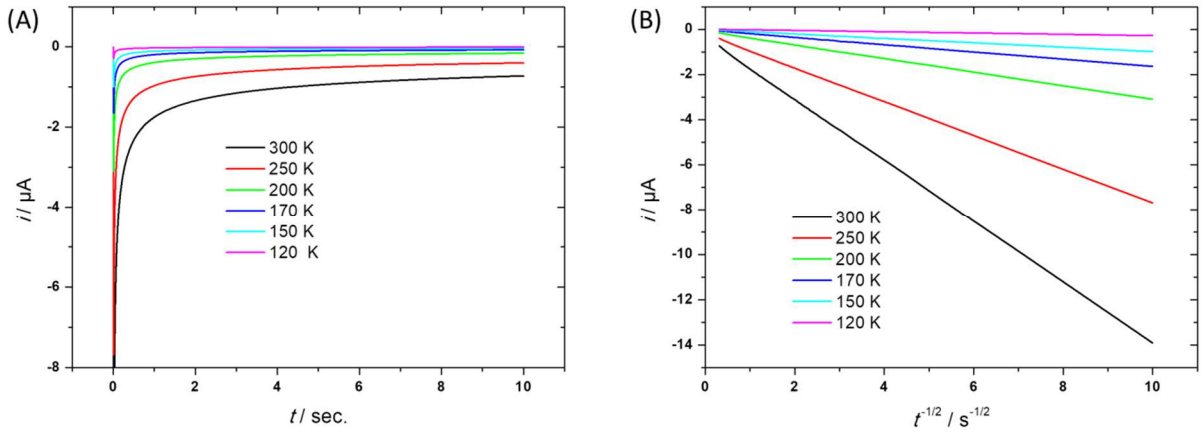

Figure 3. A) Simulated chronoamperograms and B) Resulting Cottrell plots illustrating the effect of temperature on the shape of the CAs for a mono-electronic process. C_{ox} = 1 mM, A = 0.01 cm^2. Values of $D_{ox} = D_{red}$ have been calculated for each temperature assuming that $\Delta H_D^{\neq}$ = 0.13 eV and A'_D = 0.01 cm^2 s^{-1} [27]. Simulations were carried out with the software Kissa-1D [40].

Another parameter of importance for chronoamperometry measurements at low temperatures is the cell time constant, $R_{unc}C_d$ which corresponds to the minimum time necessary to charge the double layer and, consequently, apply the requested potential. In reality, effective potential application occurs for ten times the cell time constant. Imposing a potential step on a time scale shorter than $10R_{unc}C_d$ is meaningless since the real potential applied will not correspond with the desired one. The cell time constant can be expressed as in equation (26), by using solution conductivity κ (in Ω^{-1} cm^{-1}), electrode radius r_0 (in cm) and specific differential capacitance C_d^0 (in F cm^{-2}) [24]:

$$\boldsymbol{R_{unc}C_d = \frac{r_0 C_d^0}{4\kappa}} \qquad (26)$$

Typically, cell time constant for classical (1 mm diameter) electrodes at room temperature are given around 30 µs, meaning that the lower limit of time scale in step experiments is 0.3 ms. When T decreases, the uncompensated resistance R_{unc} largely increases (due to the lowest conductivity κ) , hence inducing a significant rise of the cell time constant since double layer capacitance is poorly affected by temperature. For example, R_{unc} was found to increase by approximatively 50 times when varying the temperature from 298 K to 150 K. As a consequence, the cell time constant increases by the same factor, yielding a 1.8 ms minimum interval for step measurements. According to equation (26), one practical way to reduce this effect is to use electrodes having a smaller radius, such as ultramicroelectrodes ($r_0 \approx$ 1-10 µm). Such approach has been for instance well used for cryoelectrochemical studies on electrodes at temperatures below 100 K in liquid electrolytes [9, 41, 42].

A last, an important parameter which may induce unexpected effects for low-T chronoamperometry measurements is the diffusion layer thickness. In usual room-temperature measurements, this parameter varies from several micrometers to tens micrometers, for measurements time ranging from 1 to 10 s, according to a $(Dt)^{1/2}$ trend. Consequently, the large value of the diffusion layer compared to the roughness of a polished electrode (typically around 1 µm) allows neglecting imperfections on the electrode surface, and considering it as flat. Since diffusion coefficient values decrease with T (roughly by 100 times over 100 K), the thickness of the diffusion layer may become close to roughness of the electrode even at moderate time (10 s). Hence, measurements have to be taken and analyzed over longer time periods.

Other techniques such as chronocoulometry and double-step chonoamperometry can be used for low-T measurements. Chronocoulometry displays two main advantages *vs*. chronoamperometry: (i) it yields a signal which grows with time, hence a better signal to noise ratio at long time scale; (ii) it allows distinction between double-layer charging and faradaic currents. The charge $Q(t)$ accumulated for the potential step is expressed by the equation (27) obtained from equation (26) [24]:

$$\boldsymbol{Q(t) = \frac{2nFADC}{\pi^{1/2}} t^{1/2}} \qquad (27)$$

The diffusion coefficient can be obtained by plots of $Q(t)$ *vs*. $t^{1/2}$. As done for chronoamperometry, the variation of D with T according to an Arrhenius law yields the activation enthalpies and the pre-exponential factor for diffusion.

Double chronoamperometry (CA) is a potential step technique which is often used to extract kinetic data from chemical-coupled electrochemical reactions. The principle is to start with a classical chronoamperometry sequence (a single potential step from E_{i} to E_{f}). After a defined time τ of application of E_{f}, the potential is stepped to a new value E_{r}, allowing the electrochemical oxidation or reduction of the formed species. Of course, the value of τ determines the amount (concentration) of the various generated species within the diffusion layer. A particular case occurs when the value of E_{r} corresponds to a potential on a diffusion plateau such that it is inverse to E_{f} relative to $E^{0\prime}$ as shown in Figure 4. In that situation, the current $i_{\mathrm{r}}(t)$ which is measured upon application of E_{r}, is expressed as shown in equation (28) [24]:

$$-\boldsymbol{i}_{\mathrm{r}}(\boldsymbol{t}) = \frac{\boldsymbol{nFACD}^{1/2}}{\boldsymbol{\pi}^{1/2}}\left[\frac{\mathbf{1}}{(\boldsymbol{t}-\boldsymbol{\tau})^{1/2}} - \frac{\mathbf{1}}{\boldsymbol{t}^{1/2}}\right] \qquad (28)$$

The ratio of the reverse to the forward currents, $-i_{\mathrm{r}}/i_{\mathrm{f}}$, allows elimination of the $AD^{1/2}$ factor. If one defines t_{r} and t_{f} as times of measurement such that $t_{\mathrm{r}} - \tau = t_{\mathrm{f}}$, then the ratio can be expressed as in equation (29):

$$\frac{-\boldsymbol{i}_{\mathrm{r}}}{\boldsymbol{i}_{\mathrm{f}}} = \mathbf{1} - \left(\mathbf{1} - \frac{\boldsymbol{\tau}}{\boldsymbol{t}_{\mathrm{r}}}\right)^{\mathbf{1/2}} \qquad (29)$$

The Figure 4 displays the variation of $-i_{\mathrm{r}}/i_{\mathrm{f}}$ with t_{r}/τ. This ratio decreases asymptotically towards 0 as t_{r} increases. It equals the value of 0.293 when $t_{\mathrm{r}}/\tau = 2$ for a typical electrochemical reaction. Any deviation from this value when performing experiments is an indicator of further chemical processes occurring.

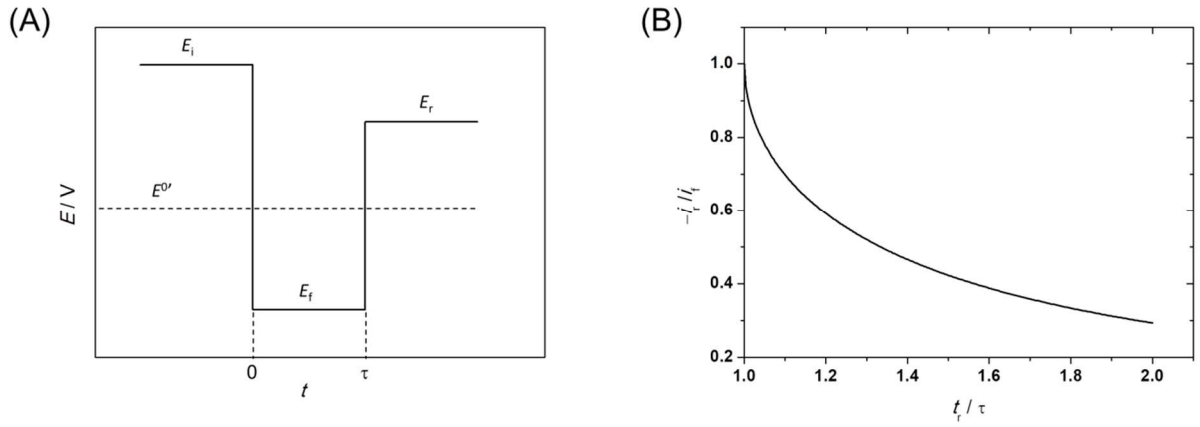

Figure 4. A) General waveform for a double potential step experiment for a reduction process and B) resulting variation of $-i_{\mathrm{r}}/i_{\mathrm{f}}$ *vs.* t_{r}/τ.

Hence, for a classical electrochemical process, this technique has a poor interest since most of the information can be obtained from a single step experiment. However, the method becomes interesting if one or several chemical reactions follow (or are concerted with) the first electrochemical event. One particular advantage is that short time kinetics can be obtained since hundreds of µs to few ms are available by step techniques. Ultra-rapid chemical processes ($k > 10^8$ s^{-1}) are no always detectable at room temperature despite the short time window of this reversal chronoamperometric. Decreasing temperature allows a significant decrease of the rate of chemical and electrochemical processes. Since chronoamperometry analysis is not affected by the kinetics of electron transfer, as long as the applied potential remains in the diffusion-controlled zone, access to the kinetics of the chemical reactions is then possible when coupling low-*T* to the double-step potential techniques.

An illustrating example of the interest of double potential chronoamperometry at low temperatures to assess chemical reactions following up electron transfer processes was reported by Birke and co-workers [43]. The rate constant for the reductive cleavage of the Co-C bond from methylcobalamin, a cofactor found in several mammalian and prokaryotic enzymes, could be calculated by double CA at temperatures between 193 and 273 K, and in two different mixtures of DMF/MeOH as solvents. An increase for the rate of the chemical reaction

occurred after increasing the content in DMF from 40% to 50% volume. Further information about double potential chronoamperometry can be found in several articles and books [24, 26].

3.3. A.C. impedance and a.c. voltammetry

A.C. impedance, also coined as electrochemical impedance spectroscopy (EIS) consists in applying an a.c. potential $\boldsymbol{V}$ of small-amplitude (V_0), superimposed on a constant d.c. bias, to the electrochemical cell and measuring the induced a.c. current $\boldsymbol{I}$ (magnitude I_0 and phase ϕ with respect to voltage) as a function of the a.c. frequency ω. The superimposed d.c. potential is used to set up the surface concentrations such that they appear as bulk values to the a.c. perturbation.

The impedance $\boldsymbol{Z}$ is intrinsically defined as resulting from the ratio of the voltage $\boldsymbol{V}$ and current $\boldsymbol{I}$ vectors, as expressed in equation (30),

$$\boldsymbol{Z} = \frac{\boldsymbol{V}}{\boldsymbol{I}} = |\boldsymbol{Z}|\exp[-\mathrm{j}\boldsymbol{\phi}] = |\boldsymbol{Z}|\cos\boldsymbol{\phi} - \mathrm{j}|\boldsymbol{Z}|\sin\boldsymbol{\phi} \qquad (30)$$

where $|\boldsymbol{Z}|$ is the modulus of $\boldsymbol{Z}$ ($|\boldsymbol{Z}| = \boldsymbol{V_0}/\boldsymbol{I_0}$) (31)

For an electrochemical cell, $\boldsymbol{Z}$ can be modelled in terms of a circuit of resistors and capacitors. The classical circuit contains a series of two parallel RC circuits representing bulk (R_{unc},C_{s}) and interfacial (R_{ct}, C_{d}, Z_{W}) properties (Figure 5). These elements correspond to the uncompensated solution resistance R_{unc}, the bulk solution capacitance C_{s}, the charge-transfer resistance R_{ct}, the double-layer capacitance C_{d}, and a 'frequency–dependent' resistance to diffusion Z_{W}, termed the Warburg impedance. The evaluation of R_{ct}, C_{dl}, R_{unc} and C_{s} is possible if the two parallel RC circuits have significantly different time constants, which is generally the case because bulk and interfacial resistance and capacitance values differ notably. From the values obtained by experimental use of a frequency response analyzer, which is able to separate the real from the imaginary part of the total impedance, a plot of Z'' against Z' ("a complex-plane plot" or "Nyquist plot") gives access to R_{ct}, C_{dl}, R_{unc} and C_{s}. Thus, the main advantage of the a.c. impedance technique is that one may determine the charge-transfer resistance and double-layer capacitance independently of the solution resistance and the bulk capacitance from the experimental value of $\boldsymbol{Z}$ as a function of ω. The complex-plane plot displays the general shape shown in Figure 5 for an equivalent circuit with pure resistors and capacitors.

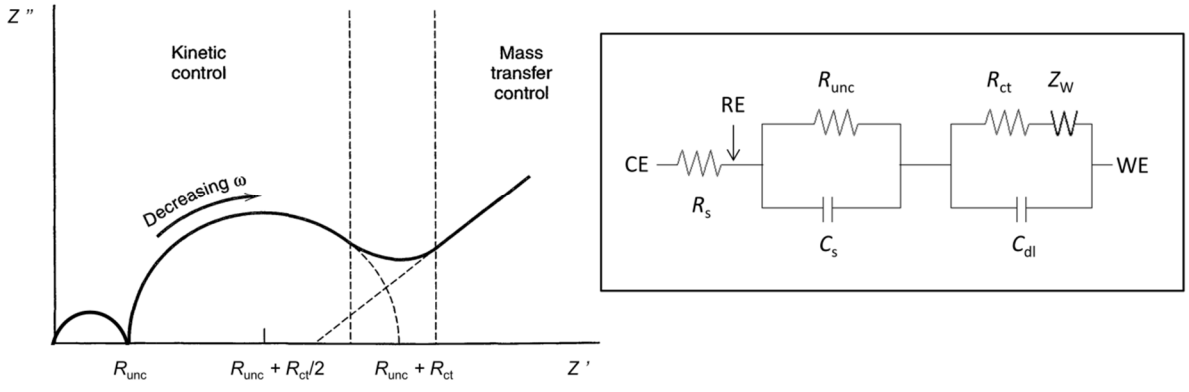

Figure 5. Complex-plane plot for an electrochemical cell (left) according to the equivalent circuit shown on the right. RE: Reference electrode; CE: Counter electrode; WE: Working electrode.

The graph can be divided into three frequency regions. At low frequencies, the Warburg impedance becomes predominant (diffusion control) and the relation between Z'' and Z' becomes linear as observed on the complex-plane plot ("Mass transfer control" region in Figure 5). Diffusion coefficients can be derived from a parameter σ which is calculated from the value of the real impedance when Z'' = 0, knowing R_{ct} and C_d.

$$\boldsymbol{Z' = Z'' - R_{unc} - R_{ct} + 2\sigma^2 C_d} \qquad (32)$$

where

$$\boldsymbol{\sigma = \frac{RT}{n^2F^2A\sqrt{2}}\left(\frac{1}{D_{ox}^{1/2}C_{ox}^{*}} + \frac{1}{D_{red}^{1/2}C_{red}^{*}}\right)} \qquad (33)$$

As the frequency increases, the Warburg impedance becomes unimportant relative to the charge-transfer resistance (kinetic control). Moreover, if the frequency is not so high as to enter the bulk parameters region, the real and imaginary components of the total impedance in the kinetic region are related as described by the equation (54):

$$\boldsymbol{\left(Z' - R_{unc} - \frac{R_{ct}}{2}\right)^2 + (Z'')^2 = \left(\frac{R_{ct}}{2}\right)^2} \qquad (34)$$

Complex-plane plot yields a semi-circle centered at $(R_{unc} + R_{ct}/2)$ on the real impedance axis and having a radius of $(R_{ct}/2)$. The maximum of this arc is at a frequency given by $1/R_{ct}\,C_d$, enabling C_d to be calculated. At even higher frequencies, only bulk properties are observed and R_{ct} and C_d can be neglected. In this region, the complex-plane plot is a semi-circle, centered at $(R_{unc}/2)$ on the real impedance axis and having a radius of $(R_{unc}/2)$. The arc has a maximum at a frequency given by $1/R_{unc}\,C_s$.

In summary, a.c. impedance gives the possibility of separating interfacial and bulk properties, which is not the case for cyclic voltammetry. This aspect is of particular interest for low-temperature studies, since the accuracy of the analysis for the study of charge-transfer kinetics is greatly improved. It is also a small-amplitude technique, which simplifies the calculations of the standard heterogeneous electron transfer constant from the charge-transfer resistance:

$$\boldsymbol{R_{ct} = \frac{RT}{nFi_0} = \frac{RT}{n^2F^2Ak^0C_{Ox}^{*(1-\alpha)}C_{Red}^{*(\alpha)}}} \qquad (35)$$

The technique is of particular interest when surface concentrations in Ox and Red species are equal. In that case, determination of k^0 becomes independent of α, the d.c. bias being set up as $E^{0\prime}$. However, it should be underlined that the analysis relies mainly on the validity of the model circuit. The above approximation is 'ideal'

as it considers the double-layer capacitance as an ideal capacitor, which is not true in fact (as observed experimentally). The theory can be refined by replacing some of the elements in the model circuit by 'distributed elements' such as constant phase elements (CPE) for example. Another drawback is that the technique yields little mechanistic information and is best used in tandem with cyclic voltammetry.

A relevant example illustrating the utility of EIS to determinate k^0 for an extremely temperature-sensitive electrochemical system has been recently published by Le Poul and co-workers [1]. The heterogeneous electron transfer rate constants were calculated for a redox couple involving μ-1,2-superoxoCu_2(II)/ μ-1,2-peroxoCu_2(II) complexes at temperatures ranging between 183 and 203 K for which the two species were stable. The variation of k^0 with temperature enabled the determination of the reorganizational energy λ value for the process.

A.c. voltammetry is an electrochemical technique derived from a.c. impedance, which can also be used for the determination of rate constant k^0 at low temperatures. It consists in applying an a.c. potential E_{ac} of low amplitude at a single frequency ω, superimposed on a linearly varying d.c. potential E_{dc} (as d.c. voltammetry). The measured responses are the magnitude of the a.c. component of the ensuing current i_{ac} at the chosen frequency of E_{ac} and its phase angle ϕ with respect to E_{ac}. One important feature to control is that time domains for the variation of E_{dc} and E_{ac} are significantly different. This can be guaranteed when the scan rate v is much smaller than the time amplitude of the a.c. potential variation, $\Delta E\omega$. Under these conditions, surface concentrations obey the Nernst equation at the potential E_{dc}. The choice of the frequency of E_{ac} is important because it defines the amplitude and shape of the resulting current. For a reversible system, the charge transfer resistance can be neglected at low frequencies and the maximum current for the bell shaped voltammetric curve is obtained at $E_{dc} = E_{1/2}$. The peak current varies with $\omega^{1/2}$. As ω increases, the charge transfer resistance becomes predominant over mass transfer (diffusion), such that the shape of the voltammogram is independent of ω. The peak current amplitude, I_{peak}, is expressed as in equation (36):

$$\boldsymbol{I}_{peak} = \frac{\boldsymbol{F^2 A k^0 C^*_{Ox} \Delta E \xi^\alpha \beta^\beta \alpha^\alpha}}{\boldsymbol{RT}} \qquad (36)$$

Where $\beta = 1 - \alpha$ and $\xi = (D_{ox}/D_{red})^{1/2}$

The equation (36) indicates that even if the standard rate constant value is sufficiently high to assume that d.c. reversibility holds, the peak current amplitude can vary strongly depending on the value of k^0. For very low value of k^0 (10^{-5} cm s^{-1}) the peak is generally no longer detected. The Figure 6 displays typical a.c. voltammograms obtained for different values of k^0 (0.01 to 1 cm s^{-1}) for quasi-reversible systems.

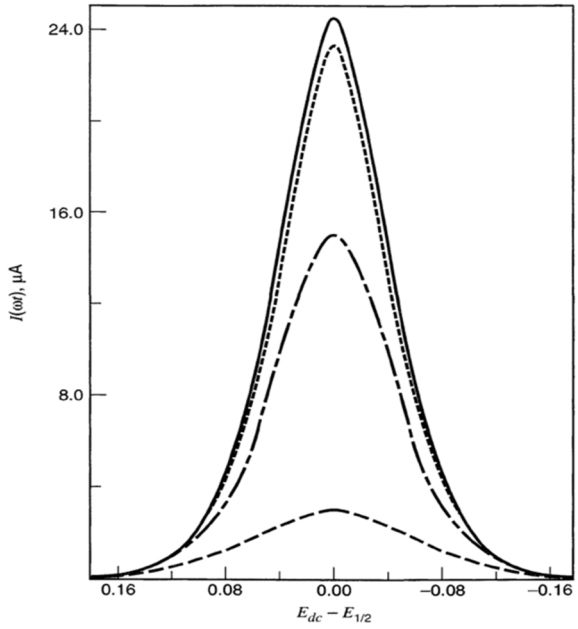

Figure 6. A.c. voltammograms for different values of k^0(1000, 1, 0.1 and 0.01 cm s^{-1} from top to bottom). Adapted from Ref. [24].

Under activation-controlled conditions (diffusion is neglected), the peak potential, E_{peak}, is centered close to $E_{1/2}$ according to the equation (37), and allows for the determination of the coefficient α:

$$\boldsymbol{E}_{\text{peak}} = \boldsymbol{E}_{1/2} + \frac{\boldsymbol{RT}}{\boldsymbol{F}} \boldsymbol{ln} \frac{\boldsymbol{\beta}}{\boldsymbol{\alpha}} \qquad (37)$$

The phase angle ϕ of the a.c. current with respect to the a.c. potential can also be a source of kinetic information. Plots of $\cos(\phi)$ *vs.* $\omega^{1/2}$ at the peak current amplitude gives the linear variation of equation (38):

$$[\boldsymbol{cos}(\boldsymbol{\phi})]_{\text{max}} = \mathbf{1} + \frac{\left(2D_{\text{Ox}}^{\boldsymbol{\beta}} D_{\text{Red}}^{\boldsymbol{\alpha}}\right)^{\mathbf{1/2}} \boldsymbol{\omega}^{\mathbf{1/2}}}{\boldsymbol{k}^{\mathbf{0}}\left[\left(\frac{\boldsymbol{\alpha}}{\boldsymbol{\beta}}\right)^{-\boldsymbol{\alpha}} + \left(\frac{\boldsymbol{\alpha}}{\boldsymbol{\beta}}\right)^{\boldsymbol{\beta}}\right]} \qquad (38)$$

From values of the diffusion coefficients and α, the standard rate constant k^0 can be directly determined from the slope of the $\cos(\phi)$ *vs.* $\omega^{1/2}$ curve. Interestingly, it was shown that equation (38) holds for any quasireversible and irreversible system (low values of k^0) even if d.c. reversibility does not apply.

In conclusion, both a.c. impedance and a.c. voltammetry methods appear thus as amongst the most appropriate and accurate electrochemical techniques to determine kinetics of electron transfer for simple reactions (no chemically coupled). Their main advantage is the separation of interfacial from bulk properties by playing with the frequency range. This makes these techniques of particular interest at low temperatures when large increase of solution resistance is obtained and disturbs the classical d.c. cyclic voltammetry. However, it should be notice that analysis of the a.c. impedance data is based on the equivalent circuit which models the electrochemical cell. The occurrence of side-reactions such as adsorption of electroactive species onto electrode surfaces or chemical processes coupled with electron transfer, may interfere in the Faradaic response, hence generating significant error in the analysis. As well, a.c. voltammetry is limited by the assumption that surface concentrations are

thermodynamically in equilibrium at E_{dc} as a consequence of the radically different timescales between the d.c potential variation and the a.c potential perturbation. When temperature is lowered, the d.c. reversibility is no longer fulfilled and severe deviations from the described theoretical framework can appear.

4. Effect of temperature on multiple electron transfers and chemically coupled electron transfers

Many electrochemical studies entail the coupling of one of several chemical reactions (C) with heterogeneous electron-transfer processes (E), particularly for reactions involving molecular species. Diverse mechanisms can be envisaged depending on the sequential or concerted occurrence of the steps, as well as their number. The most popular ones (EC, CE, EC_{cat}, ECE) have been widely discussed over several reviews and books during the last fifty years and readers are invited to refer to the literature data for detailed explanation and discussion [24, 26]. In the following sub-sections, we provide a brief description of the four mechanisms and focus our interest on the expected effect of decreasing temperature on the electrochemical signature (particularly in CV) for the different mechanisms for typical cases.

4.1. Multiple electron transfer (EE)

Since many electroactive molecules can exchange more than one electron, we will discuss in this section the electrochemical response of these species and the influence exerted by temperature on it. We will focus our analysis on changes in the shape of CVs induced by the thermodynamics and electron transfer kinetics of two electron transfer processes.

4.1.1. Thermodynamics of multiple electron transfer processes

Let us consider the case of two fast and chemically-reversible one-electron transfers for the redox couples (A/B) and (B/C) displaying $E^0_{(1)}$ and $E^0_{(2)}$ standard potentials, respectively, such that A + e^- = B and B + e^- = C (Scheme 1):

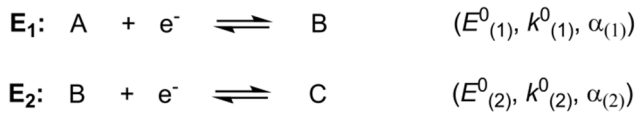

Scheme 1. EE mechanism with associated constants.

Intuitively for two successive reduction reactions involving one mono-reduced intermediate (B), electrostatics predicts that the addition of the second electron to a molecule or atom would result in a species that is more difficult to reduce. In other words, the second electron transfer reaction occurs at a potential value $E^0_{(2)}$ which is more negative than $E^0_{(1)}$ (the inverse occurs for two oxidation processes). This situation is no longer valid when significant structural changes (rearrangement of the electroactive species, large change in solvation…) are at work upon the first electron transfer, making the second one easier ($E^0_{(2)} > E^0_{(1)}$ for reduction). This case, coined as "potential inversion" is classically observed in electrochemical experiments [44]. The Figure 7 allows to

visualize the different CV responses according to the value of $\Delta E^0 = E^0_{(2)} - E^0_{(1)}$ for a reduction process, going from one two-electron process for positive values of ΔE^0 (Figure 7-A and 7-B) to two one-electron reversible systems for negative values of ΔE^0 (Figure 7-D). Whatever the situation, a disproportionation-comproportionation equilibrium 2B = A+ C involving the disproportionation constant K_{disp} and the forward/backward kinetic constants k_{disp} and k_{comp}defined in equation (39) can be considered:

$$\boldsymbol{K}_{\text{disp}} = [\text{A}][\text{C}]/[\text{B}]^{\mathbf{2}} = \boldsymbol{k}_{\text{disp}}/\boldsymbol{k}_{\text{comp}} \qquad (39)$$

The value of ΔE^0 can be thus expressed as shown in equation (60):

$$\Delta \boldsymbol{E^0} = (\boldsymbol{RT}/\boldsymbol{F})\ln \boldsymbol{K}_{\text{disp}} \qquad (40)$$

The equation (40) tells us that ΔE^0 decreases with T if one makes the rough approximation that the disproportionation reaction is temperature-independent. This indicates that the second electron transfer becomes less easy in thermodynamic terms as T diminishes. However, this effect is relatively small. For example, a temperature variation from 298 K to 175 K would lead to a 10 mV change of ΔE^0. As for monoelectronic processes, entropy effects may also induce a variation of the standard potential values, here $E^0_{(1)}$ and $E^0_{(2)}$, when the temperature is varied. One interesting example was reported by Savéant *et al.* for the reduction of polynitro compounds in order to determine the variation with T (243 K – 293 K) of the entropy and enthalpy terms for the two first successive monoelectronic transfer steps [45]. The analysis of the pseudo two-electron wave detected by CV indicated that ΔE^0 decreased linearly with T as resulting from entropic effects. More precisely, they found that the structuring of the solvent was larger for the second electron transfer than for the first one, implying that $\Delta S^0_{(1)} > \Delta S^0_{(2)}$. They also observed that the temperature variation of ΔE^0 reached 0.12 mV K^{-1} which indicated that the two redox moieties were far enough apart to behave as independent moieties.

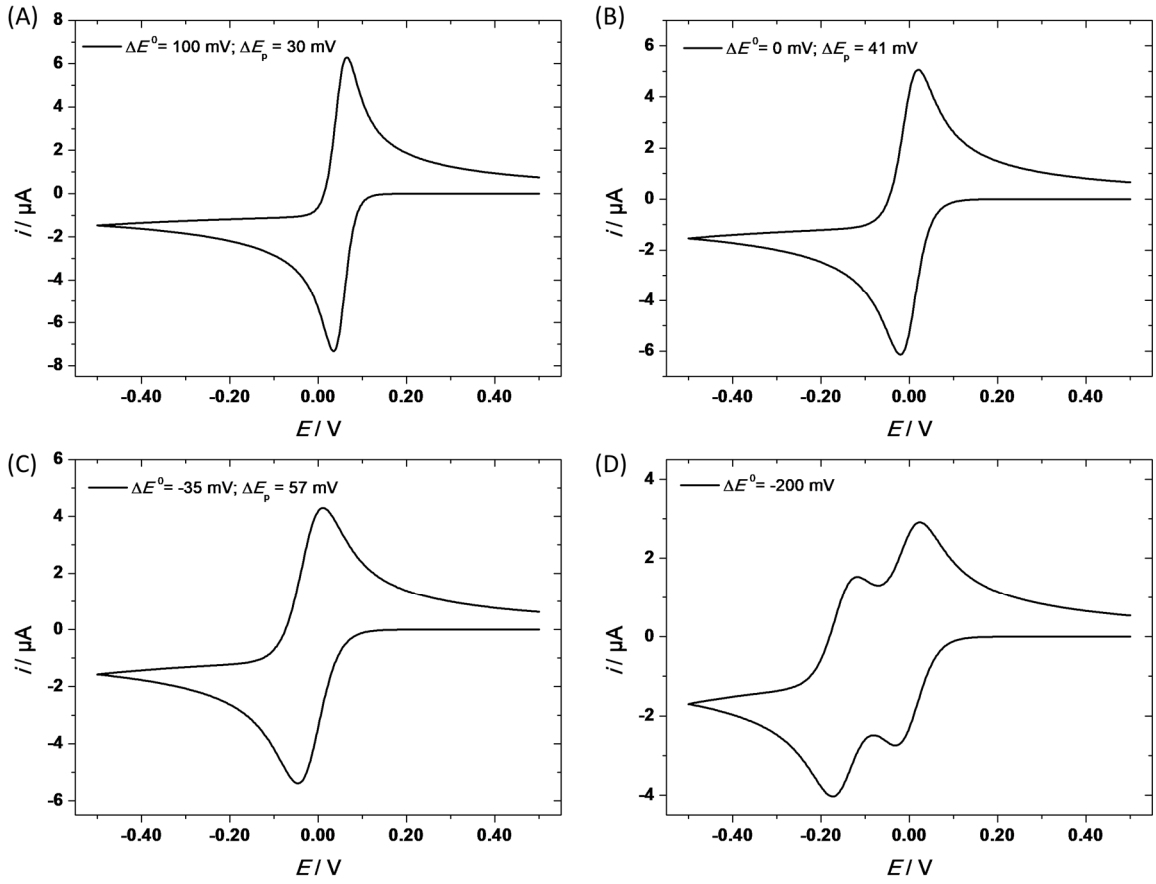

Figure 7. CV shape for different values of ΔE^0 assuming two fast electron transfers. Simulations were carried out with the software Kissa-1D [40].

One more complicate case arises when the disproportionation constant K_{disp} is temperature-dependent: if the disproportionation reaction is more favored at low T, the potential difference ΔE^0 increases. However, one could expect that this variation is relatively low since ΔE^0 varies in a logarithmic scale with K_{disp} according to the equation (40).

4.1.2. Kinetics of multiple electron transfer processes

Let us now consider the situation for which the electron transfer reactions are both reversible at room temperature, but display radically different rate constants $k^0_{(1)}$ and $k^0_{(2)}$ at low temperatures, the disproportionation reaction being slow (see below for the situation where it is fast). This case is of particular interest when the thermodynamics of both electronic transfers are equal or very similar ($E^0_{(1)} \approx E^0_{(2)}$). At room temperature, voltammetric measurements display a single system which encompasses two monoelectronic processes (see Figure 8-A) resulting from the favored disproportionation reaction and high kinetics (*vs.* mass transfer effects). At low temperature, several situations can occur depending on the ratio of the rate constants: if $k^0_{(1)}$ and $k^0_{(2)}$ are similar, a single two-electron transfer is detected but with higher peak separation and lower currents than that obtained at room temperature (Figure 8-B). Hence, the individual processes cannot be discriminated for this situation, even if the time window of the experiment is varied (through the scan rate).

However, if the ratio of the rate constants is significantly different from 1, two monoelectronic systems are detected by CV although the E^0 values remain similar (Figure 8-C). According to the Arrhenius-like equation (14), such situation may occur when either the standard free energy of activation $\Delta G^{\neq}_{0,(2)}$ or the pre-exponential factors $A'_{(2)}$ for the second process is significantly different than $\Delta G^{\neq}_{0,(1)}$ or $A'_{(1)}$, of the first process respectively. This likely happens when high reorganizational energy (solvent shell or inner sphere) is necessary to account for the second electron input to the electroactive species. Such a situation was observed by Geiger and co-workers for the oxidation of a triple-decker rhenium complex [46]: at room temperature, the complex displayed a single two-electron process whereas low-temperature (203 K) fragmented the CV curve into two waves. The authors suggested that the split could be due to (i) either slower charge-transfer kinetics for the second oxidation (*vs*. the first), leading to larger overpotentials at low *T*, (ii) or that a chemical step (isomerization) was coupled to the second electron transfer and fast enough at room temperature to induce a pseudo two-electron wave by a positive shift of the formal potential of the second ET process.

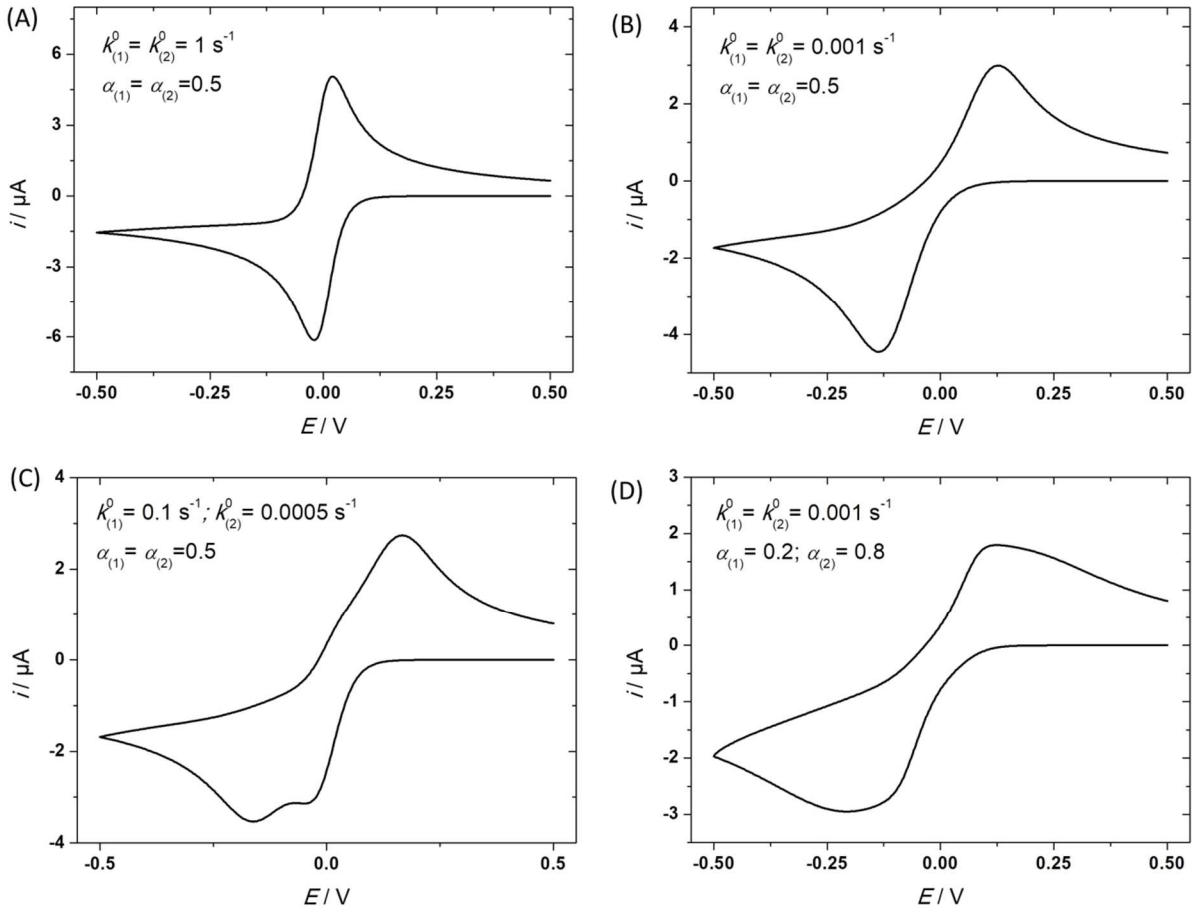

Figure 8. Simulated CVs illustrating the effect of the parameters $k^0_{(1)}$, $k^0_{(2)}$, $\alpha_{(1)}$ and $\alpha_{(2)}$ on the shape of the voltammogram for two mono-electronic processes having identical standard potentials ($E^0_{(2)} = E^0_{(1)}$). Simulations were carried out with the software Kissa-1D [40].

Another interesting case arises when the symmetry coefficients $\alpha_{(1)}$ and $\alpha_{(2)}$ for the redox processes display different values while $k^0_{(1)} = k^0_{(2)}$. While not detectable at room temperature, such differences can be observed when the electron transfer reactions become under kinetic control, such as occurring at low temperature. The Figure 8-D depicts one example of two slow mono-electronic processes occurring at $E^0_{(1)} = E^0_{(2)}$, for which $\alpha_{(1)}$ = 0.2 and $\alpha_{(2)}$= 0.8. The resulting CV displays two discernible peaks on both oxidation and reduction scans in contrast with the CV for $\alpha_{(1)} = \alpha_{(2)}$= 0.5 (Figure 8-B).

When the rates of the disproportionation/comproportionation reaction, expressed as k_{disp} and k_{comp} in equation (39), become fast, the electrochemical response is impacted because the mono-reduced species B is unstable within the timescale of the experiment. For instance, when $k^0_{(1)}$ is high and $k^0_{(2)}$ is low, the intensity of the second redox system shown in the CV of Figure 8-C vanishes in profit to a single pseudo-two-electron transfer. Theoretical and experimental examples discussing the influence of the disproportionation reaction for a EE process can be found in the literature [44, 47].

4.2. EC mechanism

The EC mechanism is defined as the sequential occurrence of an electrode electron transfer **E** with a first-order (or pseudo-first-order) follow-up homogeneous reaction **C** as shown in Scheme 2:

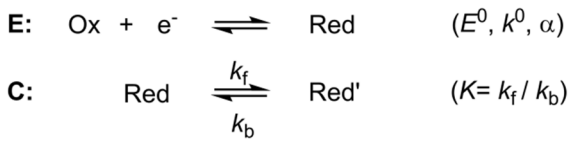

Scheme 2. EC mechanism with associated constants.

Various cases can be considered depending on the rate determining step (rds) of the mechanism. When the electron transfer is fast, the rds is the chemical reaction if one neglects diffusion. In that case, the electrochemical signature depends then on the equilibrium constant K and the rate constant $k(= k_f + k_b)$ of the chemical reaction. Often, the first-order kinetic constant is considered over a dimensionless parameter λ_{kin} (not to be misled with the reorganizational energy λ) to account for competition between the chemical reaction and diffusion (controlled by the scan rate), according to equation (61) [26]:

$$\boldsymbol{\lambda}_{\text{kin}} = \frac{\boldsymbol{RT}}{\boldsymbol{nF}}\frac{\boldsymbol{k}_f+\boldsymbol{k}_b}{\boldsymbol{v}} = \frac{\boldsymbol{RT}}{\boldsymbol{nF}}\frac{\boldsymbol{k}}{\boldsymbol{v}} \qquad (41)$$

A well-known case occurs when values of K and λ_{kin} are large, leading to “pure kinetic” conditions. This situation corresponds to a chemical reaction which is both thermodynamically and kinetically favored. In this scenario, the peak potential in cyclic voltammetry depends on the value of the forward rate constant k_f. Moreover, the expression of the peak current is close to that of the classical reversible case (Randles-Ševčik equation, see equation (21)) and varies with $v^{1/2}$. However, the system is fully irreversible (no return peak) because the forward chemical reaction occurs more rapidly than the back electron transfer reaction. In addition, K is so large that the rate of the backward chemical reaction remains lower than the timescale of the

measurement. Of course, increasing v decreases λ_{kin}, such that at some point, the experiment time scale is in competition with the rate of the forward reaction. In the limiting situation, high scan rate, the chemical reaction cannot proceed and a simple and reversible monoelectronic wave corresponding to the redox system appears in the CV.

The decrease of the temperature may impact mass transfer (diffusion coefficients D_{ox}, D_{red}), electron-transfer (E^0, k^0, α) as well as the chemical reaction (K, k). Since many different cases can occur depending on the variation of these parameters with T, we have only focused here on the situation for which the EC process is under pure kinetic conditions at room temperature and moderate scan rate. Furthermore, it is assumed that the electron transfer remains relatively fast and the chemical reaction irreversible (K large) at low temperatures. For that purpose, we have simulated cyclic voltammograms to better visualize the effect of temperature. Figure 9-A shows one CV at v = 0.1 V s^{-1} for an EC reduction process as in Scheme 2 in pure kinetic conditions at 300 K. The values of the parameters have been chosen to fit to this situation in a realistic manner: $D_{ox} = D_{red}$ = 10^{-5} cm^2 s^{-1}; k^0 = 1 cm s^{-1}; K = 100; k_f =100 s^{-1}; Assuming that a change from 300 K to 200 K leads to the following values, which are still realistic [31]: $D_{ox} = D_{red}$ = 10^{-7} cm^2 s^{-1}; k^0 = 0.001 cm s^{-1}; K = 100; k_f =0.1 s^{-1}, the CV turns from an irreversible system to a more reversible signature since an oxidation peak starts being detected at 0.1 V s^{-1} (Figure 9-C). The system is no longer under pure kinetic conditions. The effect is due to the decrease of k_f. Indeed, a smaller or larger variation of D does not affect the CV shape. Moreover, a larger decrease of k^0 does not lead to reversibility, but rather induces a negative shift of the peak potential as well as a decrease of the peak current. Hence, a 100-fold drop of the kinetics of the chemical reaction can deeply impact the voltammetric response. Higher decrease of λ_{kin} induces more reversibility to the system, which can be fully attained when $\lambda_{kin} \leq 0.16$. The effect of T is even more pronounced when using higher scan rate (1 V s^{-1}) as shown in Figure 9-B and Figure 9-D.

It is worth noting that a significant decrease of the chemical thermodynamic constant K with temperature may also impact the electrochemical signature of the EC process. For instance, a change from K = 100 to 0.1 with k_f varying from 100 to 0.1 s^{-1} leads to an increase of the reversibility of the system in terms of anodic/cathodic current ratio. The chemical conversion of the Red species in Scheme 2 is so slow (*vs*. scan rate timescale) that a small fraction of Red is transformed in Red'. In the inverse case, a raise of the thermodynamic constant while T and k_f decrease, does not affect the CV response, since the process remains limited by the sluggishness of the forward rate constant.

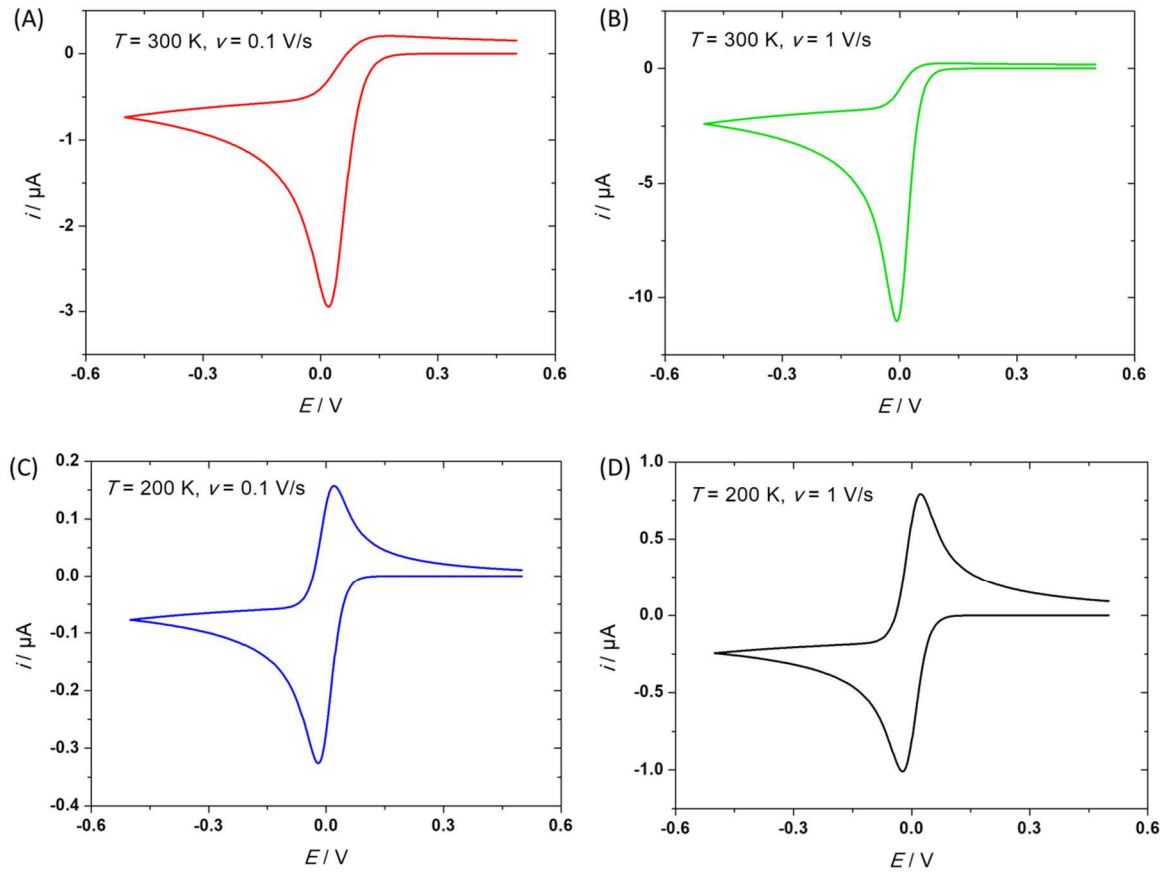

Figure 9. Effect of temperature and scan rate on voltammetric signature for an EC mechanism. A) 0.1 V s^{-1} and B), 1 V s^{-1} : T = 300 K, C_{ox} = 1 mM, D_{ox} = D_{red} = 10^{-5} cm^2 s^{-1}, k^0 = 1 cm s^{-1}, K = 100; k_f =100 s^{-1}; C) 0.1 V s^{-1} and D) 1 V s^{-1} : T = 200 K, C_{ox} = 1 mM; D_{ox} = D_{red} = 10^{-7} cm^2 s^{-1}; k^0 = 0.001 cm s^{-1}; K = 100; k_f =0.1 s^{-1}. Simulations were carried out with the software Kissa-1D [40].

An example of such situation can be found in the literature on the electrochemical reduction of monomeric Rh(III) porphyrins [48]. CV at room temperature displayed an irreversible reduction peak corresponding to the monoelectronic reduction followed by a dimerization process. In contrast, low-temperature CV (195 K) led to the detection of a reversible system, because the chemical reaction was slowed down. Another relevant example was reported by Compton and co-workers [49]. The electrochemical reduction of [(3-([trans-4-(methoxymethoxy)cyclohexyl]oxy)propyl)-sulfonyl]benzene was studied with chronoamperometry, exhaustive electrolysis and fast cyclic voltammetry at room and low temperatures. The experiments were in agreement with an EC mechanism in which the irreversible homogeneous chemical reaction consists in the cleavage of the alkyl-S bond of the radical anion. The kinetic constant, k_f, of the chemical process could be calculated at different temperatures from digital simulations of the CV curves, evidencing a striking decrease of the reaction rate at low temperature (k_f = 9000 and 300 s^{-1} at 296 and 253 K, respectively). Other examples of low-T studies of EC processes can be found in other reported contributions [16, 50-52].

4.3. CE mechanism

In the CE mechanism, a first-order (or pseudo-first-order) homogeneous reaction **C** precedes an electrode electron transfer process **E** as shown in Scheme 3:

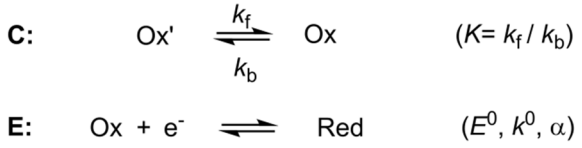

Scheme 3. CE mechanism with associated constants.

As for the EC case, the dimensionless parameter λ_{kin} accounts for the competition between the chemical reaction and the scan rate according to equation (41). Obviously, large values of the thermodynamic constant K leads to the typical wave of a reversible and monoelectronic process corresponding to the electron transfer step whatever λ_{kin}. However, small values of K produce three different situations depending on the value of λ_{kin}. In the first scenario, a low value of λ_{kin} is considered, which means that the chemical reaction is slow or the scan rate of the CV experiment is high. Under this assumption, the CV curve exhibits electrochemically reversible waves characterized by a low current, which is a function of the constant K. Increasing the value of parameter λ_{kin}, by considering a faster reaction or decreasing the scan rate, yields a new electrochemical response in which the CV curve displays a single S-shaped forward wave. The current at the plateau is then defined as a function of the rate constant k and the thermodynamic constant K, as shown by the equation (42), which describes a steady-state regime [24]:

$$\boldsymbol{i}_{\text{plateau}} = \boldsymbol{nFAC}_{\text{Ox}}\boldsymbol{KD}_{\text{Ox}}^{\boldsymbol{1/2}}\boldsymbol{k}^{\boldsymbol{1/2}} \qquad (42)$$

The rate constant k can be evaluated from the half-peak potential (of the plateau) $E_{1/2}$ knowing the standard potential value of the Ox/Red couple, as shown by the equation (43):

$$\boldsymbol{E_{1/2}} = \boldsymbol{E}^{\boldsymbol{0}}_{\text{Ox/Red}} - \boldsymbol{0.277}\frac{\boldsymbol{RT}}{\boldsymbol{nF}} - \frac{\boldsymbol{RT}}{\boldsymbol{2nF}}\ln \boldsymbol{\lambda}_{\text{kin}} \qquad (43)$$

Further increasing the value of λ_{kin} recovers partially the apparent electrochemical reversibility of the waves in the CV curve. In that diffusion-controlled zone, the thermodynamic constant K can be determined form the standard potential of the new reversible system (Ox'/Red):

$$\boldsymbol{E}_{\text{Ox'/Red}} = \boldsymbol{E}^{\boldsymbol{0}}_{\text{Ox/Red}} + \frac{\boldsymbol{RT}}{\boldsymbol{nF}}\ln \boldsymbol{K} \qquad (44)$$

As for the EC case, decreasing T may lead to many different situations. If one assumes the steady state regime at room temperature, and that kinetics of electron transfer are fast enough to avoid an impact on the total rate at any temperature, a T decrease will mainly affect D, k and K. Figure 10 exhibits simulated CVs at v = 0.1 V s^{-1} for a CE reduction process for two different temperatures, 300 K (Panel A) and 200 K (Panel B). The value of K = 0.001 and k_f = 0.1 s^{-1} have been chosen such that the system is under pure kinetic conditions at 300 K, i.e. with an S-shape forward wave. The values of the other parameters (D_{ox} = D_{red} = 10^{-5} cm^2 s^{-1}; k^0 = 1 cm s^{-1}) are as given for the EC process. The change of the temperature from 300 K to 200 K has mainly two effects. Assuming

that k_f = 0.001 s^{-1} and K keeps constant at 200 K, the plateau-shaped of the forward wave disappears and becomes peak-shaped as the forward chemical reaction is not fast enough to maintain the steady-state regime. Moreover, the system is shifted towards more positive potential as resulting from the effect of K as previously discussed for low value of λ_{kin}. If one assumes a decrease of the electron transfer kinetics at low temperature, for instance that k^0 = 0.001 cm s^{-1} rather than 1 cm s^{-1} at 200 K, one observes an increase of the peak-to-peak separation, as well as a decrease of the backward peak current (Figure 10-B).

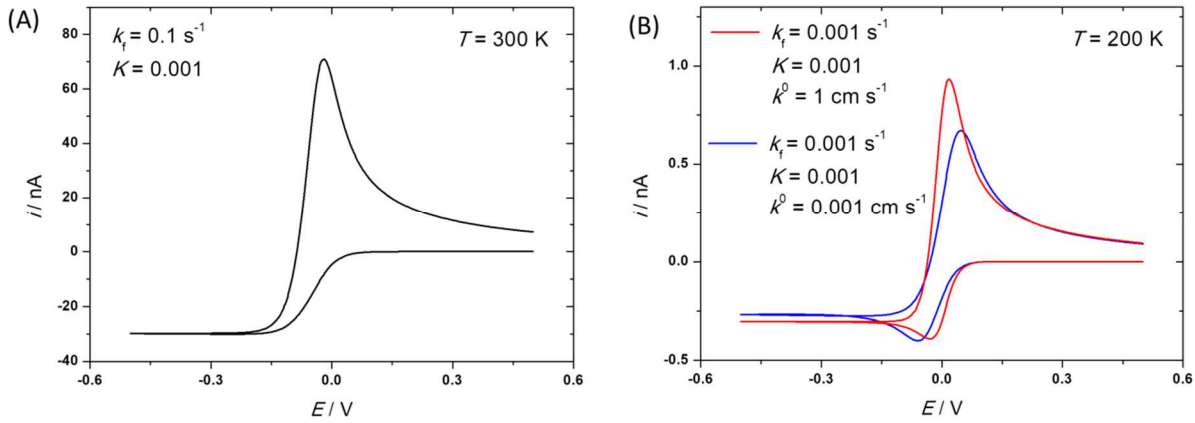

Figure 10. Effect of temperature on the voltammetric signature (v = 0.1 V s^{-1}, C_{ox} = 1 mM) for a CE mechanism. A) T = 300 K, D_{ox} = D_{red} = 10^{-5} cm^2 s^{-1}, K = 0.001; k_f =0.1 s^{-1}; B) T = 200 K, D_{ox} = D_{red} = 10^{-7} cm^2 s^{-1}, K = 0.001; k_f =0.001 s^{-1}; k^0 = 1 cm s^{-1} (red) and 0.001 cm s^{-1} (blue). Simulations were carried out with the software Kissa-1D [40].

Obviously, the variation of the thermodynamic constant K with temperature also impacts the CV shape. A decrease of K with T (and k_f) would favor formation of the Ox' species over Ox. Consequently, the redox system would return back to the pure kinetic conditions with the formation of a plateau shape curve in CV, but with a lower current intensity. For instance, a 10-fold decrease of K from 0.001 to 0.0001 would be sufficient to consider the change of kinetic regime and the observation of a S-shaped CV (not shown). Inversely, an increase of K while T decreases would affect the electrochemical signature in the other way since the system would rather evolve toward a peak-shaped CV of higher current intensity.

An example of a low-temperature electrochemical study of a molecule involving a CE mechanism was published by Bowyer and Evans in 1988 [53]. In their study, CV experiments on a solution of *trans*-1,2-diiodocyclohexane were carried out at temperatures ranging between 273 and 233 K. This organic compound presents two conformational structures in equilibrium: an axial-axial conformer, which is thermodynamically favored, and an equatorial-equatorial conformer. Interestingly, each conformer gave two distinct and separated voltammetric waves which could be analyzed by digital simulation of the curves. Hence, the thermodynamic parameters of the conformational chemical equilibrium could be calculated leading to values in agreement with NMR measurements. The electrochemical behavior of *trans*-1,2-diiodocyclohexane did not fit exactly a CE mechanism as the two species involved in the preceding chemical reaction, i.e. Ox and Ox', were electrochemically active.

4.4. EC_{cat} mechanism

The EC_{cat} mechanism is a particular case of an EC mechanism in which the homogeneous chemical reaction is a catalytic process mediated by the reduced species Red. As a result, substrate A is converted into product B, and oxidized species Ox is recovered. The Scheme 4 depicts the sequential steps **E** and $\mathbf{C_{cat}}$ of such process:

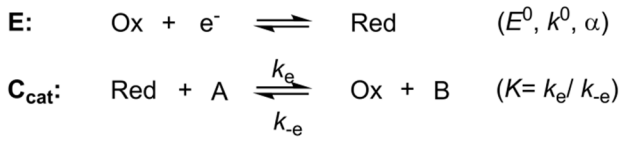

Scheme 4. EC_{cat} mechanism with associated constants.

The simplest approximation considers the chemical reaction as the rate-determining step. The electrochemical responses are then dependent on the dimensionless parameter $\lambda_e = RTk_eC_{Ox}^*/Fv$ and the excess factor $\gamma = C_A^*/C_{Ox}^*$ which is the ratio of the bulk concentrations in substrate and catalyst. High values γ and moderately high value of λ_e lead to a typical case of electrocatalysis which is characterized by a S-shaped cyclic voltammogram, whose current plateau i_{cat} is proportional to $k_e^{1/2}$, and, importantly, independent on the scan rate, as defined in equation (45) [24]:

$$\boldsymbol{i_{cat} = nFAC_{Ox}^* D_{ox}^{1/2} k_e^{1/2} (C_A^*)^{1/2}} \qquad (45)$$

At low value of γ while λ_e is large, the CV reaches a particular situation coined as "total catalysis" for which two peaks are observed in CV on the forward scan. The first peak is a substrate-diffusion-controlled catalytic process whose potential peak value (but not the current peak value) is dependent of k_e. The second peak corresponds to a catalyst-diffusion-controlled electron transfer as observed in absence of substrate A.

Since the excess factor is not expected to be temperature-dependent (or can be neglected), a decrease of *T* likely impacts λ_e, D, and electron transfer parameters (k^0, E^0, α). Similarly to the EC case, changes of the electrochemical signature with *T* can be multiple depending on how these parameters vary. The two above-mentioned specific cases (S-shape and total catalysis) have been considered by voltammetric simulations at 300 K and 200 K in order to better visualize how *T* would affect the CV response. Figure 11-A and B shows simulated CVs at 300 K for S-shaped (A) and total catalysis (B), which are differentiated by the value of the excess factor ($\gamma = 10^3$ and 1, respectively) and the forward catalytic rate constant ($k_e = 10^2$ M^{-1} s^{-1} and 10^7 M^{-1} s^{-1}, respectively), all other parameters being the same ($K = 10^5$, $D_{ox} = D_{red} = D_A = D_B = 10^{-5}$ cm^2 s^{-1}, $k^0 = 1$ cm/s, $v = 0.1$ V s^{-1}, $\alpha = 0.5$). Here, the chemical process is considered as irreversible at all temperatures, *K* being large (10^5). At 200 K, only diffusion coefficients and standard rate constants are modified as previously discussed for the EC and CE mechanisms ($D_{ox} = D_{red} = D_A = D_B = 10^{-7}$ cm^2 s^{-1}, $k^0 = 0.001$ cm s^{-1}). Assuming that k_e decreases by a 100-fold manner, significant modifications of the CVs are observed as shown in Figure 11-C and D. The S-shaped CV at 300 K disappears in profit to a reversible system (Figure 11-C), since the catalytic reaction is not fast enough to occur (*vs.* timescale of the experiment). The total-catalysis case in Figure 11-B is also modified since the pre-peak is no longer observed in Figure 11-D at 200 K. The decrease in k_e shifts the

pre-peak potential closer to the catalyst-diffusion-controlled peak. The constant is however still high enough to allow regeneration of the catalyst, as shown by the higher forward peak current *vs*. backward. One example of low-T study of an EC_{cat} mechanism was reported by Peters and co-workers in 2016 [54]. These authors investigated the binding properties of tetradente P_3^B and P_3^C iron complexes towards dinitrogen and the electrocatalytic conversion of N_2 into ammonia under acidic conditions in $Et_2O/NaBAr^F$. Studies were carried out at 228 K (-45°C) to stabilize the *in-situ*-generated Fe-N_2 adducts and to allow reactivity with strong acids, as shown by the observation of an electrocatalytic wave.

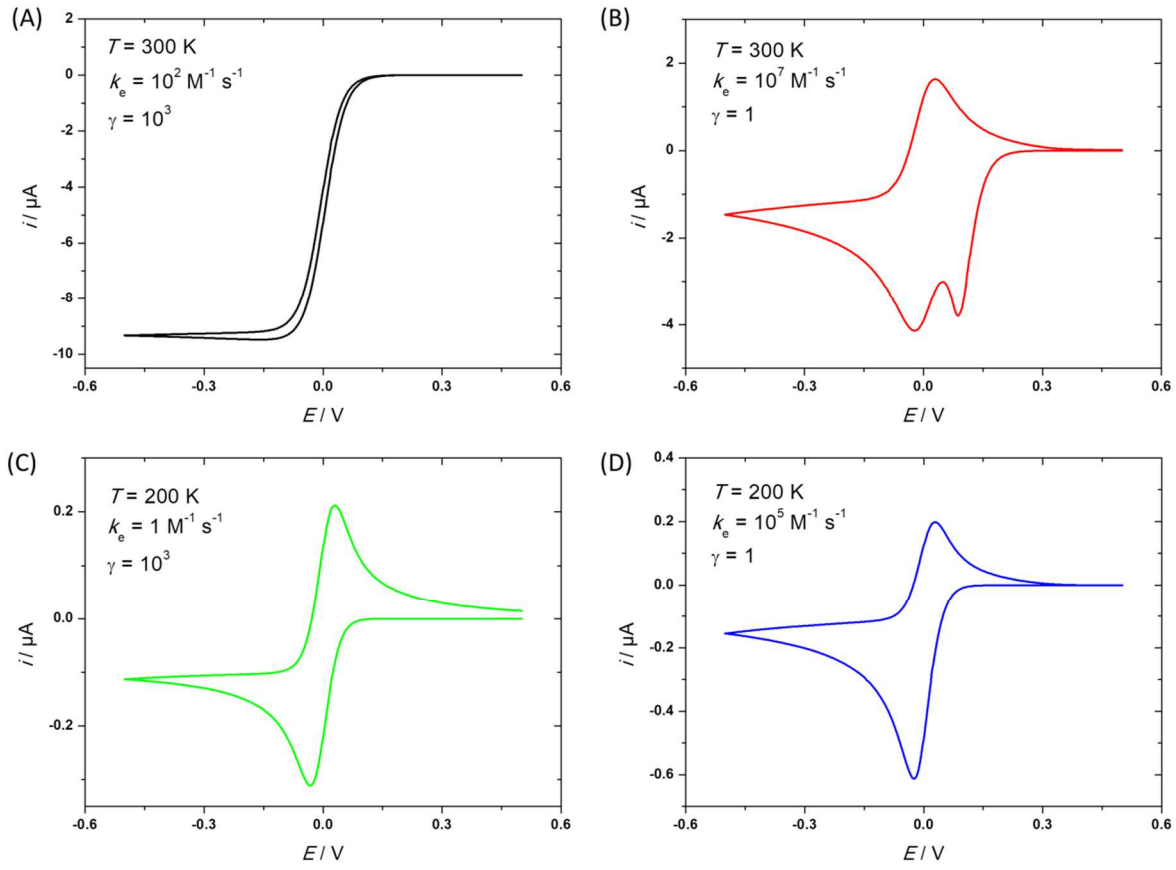

Figure 11. Effect on temperature on the voltammetric signature for an EC_{cat} mechanism. A) T = 300 K, D_{ox} = D_{red} = 10^{-5} cm^2 s^{-1}, k^0 = 1 cm s^{-1}, K = 10^5; k_e = 10^2 M^{-1} s^{-1}, γ = 10^3; B) T = 300 K, D_{ox} = D_{red} = 10^{-5} cm^2 s^{-1}, k^0 = 1 cm s^{-1}, K = 10^5; k_e = 10^7 M^{-1} s^{-1} , γ = 1; C) T = 200 K, D_{ox} = D_{red} = 10^{-7} cm^2 s^{-1}, k^0 = 0.001 cm s^{-1}, K = 10^5; k_e = 1 M^{-1} s^{-1}; γ = 10^3; D) T = 200 K, D_{ox} = D_{red} = 10^{-7} cm^2 s^{-1}, k^0 = 0.001 cm s^{-1}, K = 10^5; k_e = 10^5 M^{-1} s^{-1}; γ = 1. Simulations were carried out with the software Kissa-1D [40].

4.5. ECE mechanism

As shown in Scheme 5, the ECE mechanism corresponds to the sequential occurrence of one first electrode electron transfer $\mathbf{E_1}$, followed by first-order (or pseudo-first-order) homogeneous reaction $\mathbf{C_1}$, and a second

electrode reaction **E₂**. A supplemental reaction **C₂**, a disproportion process, can also be considered under certain circumstances (see below).

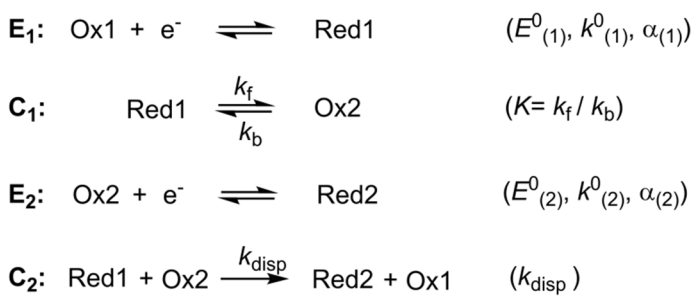

Scheme 5. ECE(C) mechanism with associated constants.

Two main situations are generally observed for the **E₁C₁E₂** mechanism, depending on the difference between the standard potentials of each microscopic electrode reaction, $\Delta E^0 = E^0_{(2)} - E^0_{(1)}$. For a reduction process, a negative value of ΔE^0 (positive for an oxidation process) implies that the **E₂** reaction is more difficult than **E₁**. In that situation, the overall reaction corresponds to two one-electron processes, the first obeying to an EC mechanism. The second case, which is of greater interest, occurs for a positive value of ΔE^0 (negative for an oxidation process) if one considers a reduction process. Thus, the second electrochemical reduction, $E^0_{(2)}$, occurs at a higher potential than $E^0_{(1)}$and a pseudo two-electron process is observed. However, the electrochemical signature depends on the values of K and k_f compared to the scan rate (timescale) and the kinetics of the electron transfer processes. The dimensionless parameter $\lambda_{kin} = RT(k_f + k_b)/Fv$ which is identical to that defined for an EC mechanism (equation (61)) allows defining the different kinetic zones. High values of λ_{kin} (hence k_f) and moderate-to-low values of K lead to the situation for which a reversible two-electron process is predominant (Ox1 + 2e$^-$ = Red2), as shown by CV in Figure 12-A (black curve, K = 10, k_f= 10^8 s^{-1}). Here, the standard potential of the Ox1/Red2 redox couple is given by the equation (46) [24]:

$$\boldsymbol{E^0}(\mathrm{Ox1/Red2}) = \frac{\boldsymbol{E^0_{(1)}+E^0_{(2)}}}{\boldsymbol{2}} - \frac{\boldsymbol{RT}}{\boldsymbol{2F}}\boldsymbol{lnK} \qquad (46)$$

When λ_{kin} decreases and K remains constant, another situation arises for which the forward chemical rate is not large enough to fully supply the species Ox2 at the electrode surface. One particular case appears when one reaches the "pure kinetic" conditions, which corresponds to an irreversible CV signature on the forward scan (see Figure 12-A, red curve, for K = 10, k_f= 10 s^{-1}). The cathodic peak current is twice that obtained for an EC process under pure kinetic conditions, and is defined by the equation (47) [26].

$$\boldsymbol{i}_p = \boldsymbol{0.992}\left(\frac{\boldsymbol{F^3}}{\boldsymbol{RT}}\right)^{\boldsymbol{1/2}}\boldsymbol{AD^{1/2}Cv^{1/2}} \qquad (47)$$

As for the others above-discussed mechanisms, the decrease of T is expected to impact the electrochemical signature in terms of mass transfer, electron transfers and chemical reactions. The Figure 12-B displays the CVs resulting from a 10^2-fold decrease of the forward rate constant k_f, without change of K, still with decrease of k^0

(from 1 to 10^{-3} cm s^{-1}) and diffusion coefficients (from 10^{-5} to 10^{-7} cm^2 s^{-1}). The pseudo two-electron reversible process which occurs at 300 K for k_f = 10^8 s^{-1} (black curve, Figure 12-A) becomes irreversible at 200 K with k_f = 10^6 s^{-1} (blue curve, Figure 12-B) as shown by the shift of the forward reduction peak towards more negative values. This is a consequence of the diminution of λ_{kin} as observed at 300 K in Figure 12-A (red curve). Indeed, for a lower value of the forward chemical rate constant k_f (10^{-1} s^{-1}), the chemical reaction becomes slow, but two oxidation peaks for species Red1 and Red 2 are still discernible. Finally, at an even lowest value of k_f (10^{-3} s^{-1}), the oxidation peak for Red 2 vanishes and a single reversible system corresponding to the reaction **E₁** is observed (orange curve, Figure 12-B), thus allowing the determination of $E^0_{(1)}$.

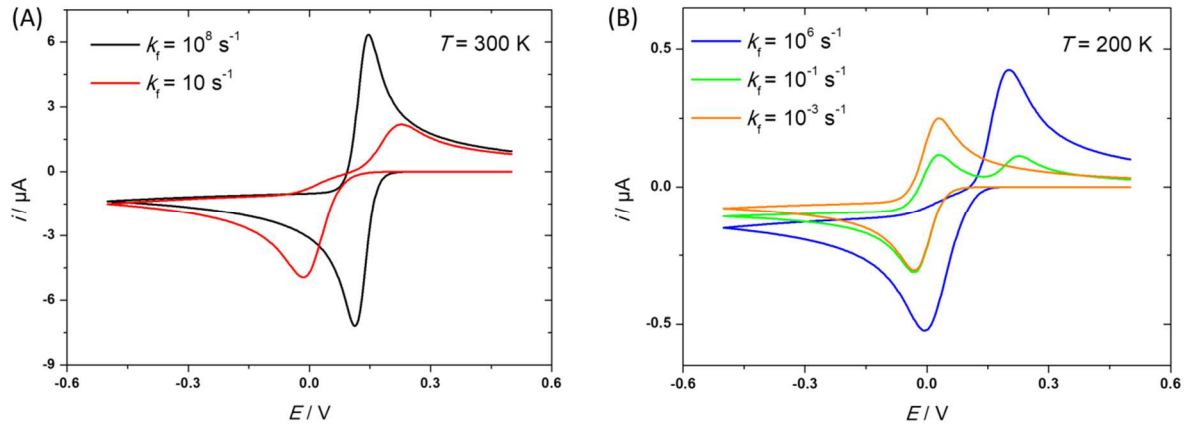

Figure 12. Effect of temperature and scan rate on voltammetric signature for an ECE mechanism with ΔE^0 being negative. A) T = 300 K, D_{ox} = D_{red} = 10^{-5} cm^2 s^{-1}, k^0 = 1 cm s^{-1}, K = 10; k_f = 10^8 s^{-1} (black curve) and k_f = 10 s^{-1} (red curve) ; B) T = 200 K, D_{ox} = D_{red} = 10^{-7} cm^2 s^{-1}, k^0 = 0.001 cm s^{-1}, K = 10; k_f = 10^6 s^{-1} (blue curve), k_f = 10^{-1} s^{-1} (green curve) and k_f = 10^{-3} s^{-1} (orange curve). Simulations were carried out with the software Kissa-1D [40].

As for the others cases, a further consideration consists in taking into account the variation of the thermodynamic constant K with temperature. If K increases when T (and k_f) decreases, the changes on the voltammetric curves are only detectable for high values of k_f (for instance k_f = 10^6 in reference to Figure 12-B, blue curve). A diminution of the current intensity for the return peak as well as a slight shift of the anodic peak potential are then observed. This effect is due to the irreversible character of the chemical reaction **C₁** in that situation which does not allow the back formation of species Ox1 on the return scan. Inversely, a decrease of K with T modifies the CV only for moderate values of k_f (here 10^{-1} s^{-1}). The ratio of the two anodic peaks on the return scan is changed in favor of the Red1-Ox1 reaction at the lowest potential because the concentration in Ox1 *vs.* Ox2 increases. A decrease of K has almost no effect when the kinetics are very fast or very slow.

A more complicated case arises when a chemical homogenous electron exchange reaction occurs between Red1 and Ox2 species near the electrode surface, as shown in Scheme 5 with reaction **C₂**. This reaction is often considered as a disproportionation-comproportionation reaction, giving rise to ECE-DISP types of mechanisms [24, 26]. The rate constant k_{disp} of this irreversible reaction can also impact substantially the electrochemical behavior, particularly when the forward rate constant k_f of the reaction **C₁** is low and k_{disp} is large. Hence, a

large decrease of k_f due to the lowering of the temperature can be eventually overcompensated by the rate of the disproportionation reaction which occurs near the electrode surface.

Several examples of low-*T* studies of ECE and more complicated ($E(C_nE_n)$) processes can be found in literature [55-59]. For example, Van Duyne and Reilley investigated the reduction of *p*-iodo-nitrobenzene by cyclic voltammetry [55]. The organic compound displayed two successive irreversible peaks at 298 K, whereas one quasi-reversible system was observed at 212 K. The low-*T* behavior was ascribed to the reversible formation of the *p*-iodo-nitrobenzyl radical anion. This radical was sufficiently stable within the timescale of the experiment to be characterized at low scan rate. At room-temperature, the poor stability of the radical induced C-I bond cleavage and hydrogen abstraction of the solvent induced formation of nitrobenzene. The latter was shown to be reduced irreversibly at a higher redox potential than *p*-iodo-nitrobenzene, thus explaining the two irreversible peaks at 298 K, as expected for a $\mathbf{E_1CE_2}$ reduction process for which $E^0_{(2)} > E^0_{(1)}$.

An interesting example of an electroactive molecule exhibiting an E_1CE_2 mechanism was reported by Sweigart and co-workers [60]. The electrochemical reduction of (Methylcyclopentadienyl)$Mn(CO)_2NO^+$ and (indenyl)$Mn(CO)_2NO^+$ complexes was analyzed by cyclic voltammetry at 296 and 230 K. A comparison of the results obtained at the two temperatures showed that reduction of the compounds produced an unstable 19-electron complex which evolved following a dissociative chemical step in which a CO ligand is released. The resulting 17-electron complex could subsequently react with nucleophiles, like PPh_3, to form a new species which was reduced at a higher standard potential than that of the initial complex ($E^0_{(2)} > E^0_{(1)}$). Although the mechanism should be properly described with an ECCE scheme, the extremely fast coordination of nucleophiles to the 17-electron complex ($k > 10^5$ M^{-1} s^{-1} at 230 K) implied that the dissociation of the CO ligand was the chemical rate-determining step. Digital simulations of the CV curves for the two complexes at 230 K allowed the calculation of the kinetic constants for the irreversible dissociation of CO at that temperature. Despite the substantial difference in electronic properties of the methylcyclopentadienyl and indenyl ligands, the kinetic constant were pretty similar ($k_{CO,\,diss.}$ = 7 and 15 s^{-1}, respectively).

5. Conclusions

In this paper, theoretical aspects of low-temperature electrochemistry have been discussed. In particular, we showed that Marcus and Marcus-DOS theoretical models of electron-transfer could finely predict the variation of heterogeneous ET kinetics with temperature on the basis of experimental data (solvent, electrolyte, electrode and redox active species physical properties). Moreover, we demonstrated that electrochemical methods (CV, CA to cite few) could provide valuable thermodynamic and kinetic data when applied to low-temperature conditions, which cannot be extracted from room temperature experiments. At last, we discussed on the effect of lowering temperature on the electrochemical responses in the particular frame of chemically-coupled electron-transfer processes (EC, ECE…) which can be found in molecular electrochemistry. For a more general point of view, this paper has emphasized that analysis of simple or complicated electron transfer reactions occurring at an electrode surface could fully benefit from the decrease of temperature in many ways. As previously stated [20], more information can be obviously obtained from measurements combining electrochemical methods to spectroscopy (UV-Vis, NIR, IR, Raman, EPR..), for *in-situ* and real time characterization of transient species, which cannot be stabilized at room temperature. Although low-*T* electrochemistry and spectroelectrochemistry remain unfrequently used nowadays, the on-going development of new spectroscopic set-ups displaying enhanced

performances in terms of time acquisition, sensitivity and handling, combined with miniaturized electrochemical systems will certainly boost low-*T* approaches in many domains (catalysis, electrochromic sensors, energy conversion…)[61].

Author information

*Corresponding authors

Isidoro López: isilopmarin@gmail.com. ORCID: 0000-0002-6014-0078

Nicolas Le Poul: nicolas.lepoul@univ-brest.fr. ORCID: 0000-0002-5915-3760

Declaration of competing interest

The authors declare no competing financial interest.

Acknowledgments

Financial support by ANR-13-BSO7-0018, Conseil Général du Finistère, Université de Bretagne Occidentale and Campus France (Prestige grant number 2015-2-0019 for I. L.-M.).

References

[1] I. Lopez, R. Cao, D.A. Quist, K.D. Karlin, N. Le Poul, Direct determination of electron-transfer properties of dicopper-bound reduced dioxygen species by a cryo-spectroelectrochemical approach, Chem. Eur. J., 23 (2017) 18314-18319.
[2] L. Rand, C.S. Rao, Electrochemical oxidation of epimeric .beta.-hydroxycycloalkylacetic acids, J. Org. Chem, 33 (1968) 2704-2708.
[3] B.G. Dekker, M. Sluyters-Rehbach, J.H. Sluyters, On the impedance of galvanic cells, J. Electroanal. Chem., 21 (1969) 137-147.
[4] F.F. Gadallah, R.M. Elfson, Arylation of aromatic compounds by electrochemical reduction of benzenediazonium tetrafluoroborate in aprotic solvents, J. Org. Chem., 34 (1969) 3339-3338.
[5] R.A. Meinzer, D.W. Pratt, R.J. Myers, Electron spin resonance spectrum of a new radical produced by the reduction of tetrasulfur tetranitride and its identification as the radical anion of tetrasulfur tetranitride, J. Am. Chem. Soc., 91 (1969) 6623-6625.
[6] R.J. Wilson, L.F. Warren Jr., M.F. Hawthorne, The existence of the nickel(IV) dication derived from nickelocene and a cationic boron hydride analog, J. Am. Chem. Soc., 91 (1969) 758-759.
[7] L.L. Miller, E.A. Mayeda, Electrooxidative rearrangement of 1,1,3-triphenyIindene in sulfur dioxide solvent, J. Am. Chem. Soc., 92 (1970) 5818-5819.
[8] R.P. Van Duyne, C.N. Reilley, Low-temperature electrochemistry. I. Characteristics of electrode reactions in the absence of coupled chemical kinetics, Anal. Chem., 44 (1972) 142-152.
[9] J.T. McDevitt, S. Ching, M. Sullivan, R.W. Murray, Fluid electrolyte solutions for electrochemistry at near liquid nitrogen temperatures, J. Am. Chem. Soc., 111 (1989) 4528-4529.
[10] S.R. Peck, L.S. Curtin, J.T. McDevitt, R.W. Murray, J.P. Collman, W.A. Little, T. Zetterer, H.M. Duan, C. Dong, A.M. Hermann, Response of the double-layer capacitance of a high-temperature superconductor/fluid electrolyte interface to the onset of superconductivity, J. Am. Chem. Soc., 114 (1992) 6771-6775.
[11] S.R. Peck, L.S. Curtin, L.M. Tender, M.T. Carter, R.H. Terrill, R.W. Murray, J.P. Collman, W.A. Little, H.M. Duan, Voltammetry of self-assembled ferroceneoctanethiol monolayers on metal-coated high-temperature superconductor electrodes at sub-Tc temperatures, J. Am. Chem. Soc., 117 (1995) 1121-1126.
[12] S.J. Green, D.R. Rosseinsky, D.C. Sinclair, A liquid-electrolyte voltammetric probe of superconducting oxocuprates through the transitions temperature Tc, J. Chem. Soc., Chem. Commun., (1994) 1421-1422.

[13] S.J. Green, D.R. Rosseinsky, D.R. Rosseinsky, A.L. Kharlanov, J. Paul Attfield, A new probe of superconductivity: quantitative measurements on defined electron transfer with solute at the interface between liquid electrolyte and oxocuprate electrode in the superconducting state, Chem. Commun., (1998) 1215-1216.
[14] S.J. Green, N. Le Poul, P.P. Edwards, G. Peacock, Sub-Tc electron transfer at the Hg-HTSC/liquid-electrolyte interface, J. Am. Chem. Soc., 125 (2003) 3686-3687.
[15] N. Le Poul, S.J. Green, J.P. Attfield, Sub-Tc electron transfer at the HTSC/polymer interface, Chem. Commun., (2003) 638-639.
[16] J.O. Taylor, G. Neri, L. Banerji, A.J. Cowan, F. Hartl, Strong impact of intramolecular hydrogen bonding on the cathodic path of [Re(3,3'-dihydroxy-2,2'-bipyridine)(CO)3Cl] and catalytic reduction of carbon dioxide, Inorg. Chem., 59 (2020) 5564-5578.
[17] M. Bubrin, D. Schweinfurth, F. Ehret, S. Záliš, H. Kvapilová, J. Fiedler, Q. Zeng, F. Hartl, W. Kaim, Structure and spectroelectrochemical response of arene–ruthenium and arene–osmium complexes with potentially hemilabile noninnocent ligands, Organometallics, 33 (2014) 4973-4985.
[18] L. Tender, M.T. Carter, R.W. Murray, Cyclic voltammetric analysis of ferrocene alkanethiol monolayer electrode kinetics based on Marcus theory, Anal. Chem., 66 (1994) 3173-3181.
[19] R.P. Van Duyne, C.N. Reilley, Low-temperature electrochemistry. II. Evaluation of rate constants and activation parameters for homogeneous chemical reactions coupled to charge transfer, Anal. Chem., 44 (1972) 153-158.
[20] I. López, N. Le Poul, Low-temperature electrochemistry and spectroelectrochemistry for coordination compounds, Coord. Chem. Rev., 436 (2021) 213823.
[21] E. Anxolabéhère, D. Lexa, M. Momenteau, J.M. Saveant, Supramolecular entropy gains: simple and superstructured iron porphyrins, J. Phys. Chem., 96 (1992) 9348-9352.
[22] Handbook of chemistry and physics 84th edition, CRC Press2003-2004.
[23] J.E. Leffler, E. Grunwald, Equilibria of organic reactions - As treated by statistical, thermodynamic, and extrathermodynamic methods, John Wiley & Sons, New York1963.
[24] A.J. Bard, L.R. Faulkner, Electrochemical methods: fundamentals and applications, Wiley2000.
[25] E.J.F. Dickinson, J.G. Limon-Petersen, N.V. Rees, R.G. Compton, How much supporting electrolyte is required to make a cyclic voltammetry experiment quantitatively "diffusional"? A theoretical and experimental investigation, J. Phys. Chem. C, 113 (2009) 11157-11171.
[26] J.-M. Savéant, Elements of molecular and biomolecular electrochemistry, John Wiley & Sons2006.
[27] J.N. Richardson, J. Harvey, R.W. Murray, Heterogeneous electron-transfer dynamics of decamethylferrocene from 130 to 181 K, J. Phys. Chem., 98 (1994) 13396-13402.
[28] M.C. Henstridge, E. Laborda, N.V. Rees, R.G. Compton, Marcus–Hush–Chidsey theory of electron transfer applied to voltammetry: A review, Electrochim. Acta, 84 (2012) 12-20.
[29] R.J. Marcus, B.J. Zwolinski, H. Eyring, The electron tunnelling hypothesis for electron exchange reactions, J. Phys. Chem., 58 (1954) 432-437.
[30] R.A. Marcus, On the theory of electron-transfer reactions. VI. Unified treatment for homogeneous and electrode reactions., J. Chem. Phys., 43 (1965) 679-701.
[31] N. Le Poul, S.J. Green, Y. Le Mest, Determination of heterogeneous electron-transfer kinetics of decamethylferrocene at low temperatures (120 K < T < 200 K) by a.c. impedance, J. Electroanal. Chem., 596 (2006) 47-56.
[32] C.E.D. Chidsey, Free energy and temperature dependence of electron transfer at the metal-electrolyte interface, Science, 251 (1991) 919-922.
[33] W. Schmickler, E. Santos, Interfacial electrochemistry 2nd Edition, Springer2010.
[34] J.N. Richardson, S.R. Peck, L.S. Curtin, L.M. Tender, R.H. Terrill, M.T. Carter, R.W. Murray, G.K. Rowe, S.E. Creager, Electron-transfer kinetics of self-assembled ferrocene octanethiol monolayers on gold and silver electrodes from 115 to 170 K, J. Phys. Chem., 99 (1995) 766-772.
[35] E. Laborda, M.C. Henstridge, C. Batchelor-McAuley, R.G. Compton, Asymmetric Marcus-Hush theory for voltammetry, Chem. Soc. Rev., 42 (2013) 4894-4905.
[36] E. Laviron, General expression of the linear potential sweep voltammogram in the case of diffusionless electrochemical systems, J. Electroanal. Chem., 101 (1979) 19-28.
[37] R.S. Nicholson, I. Shain, Theory of Stationary Electrode Polarography. Single Scan and Cyclic Methods Applied to Reversible, Irreversible, and Kinetic Systems, Anal.Chem., 36 (2002) 706-723.
[38] H.O. Finklea, D.D. Hanshew, Electron-transfer kinetics in organized thiol monolayers with attached pentaammine(pyridine)ruthenium redox centers, J. Am. Chem. Soc., 114 (1992) 3173-3181.
[39] G. Diao, Z. Zhang, Determination of heterogeneous rate constants for the electrochemical reduction of fullerene C60 by the method of cyclic voltammetry on a hemispherical ultramicroelectrode, J. Electroanal. Chem., 414 (1996) 177-181.
[40] C. Amatore, O. Klymenko, I. Svir, A new strategy for simulation of electrochemical mechanisms involving acute reaction fronts in solution: Principle, Electrochem.Commun., 12 (2010) 1170-1173.

[41] S. Ching, J.T. McDevitt, S.R. Peck, R.W. Murray Liquid Phase Electrochemistry at Ultralow Temperatures, J. Electrochem. Soc., 138 (1991) 2308-2315.
[42] S.J. Green, D.R. Rosseinsky, M.J. Toohey, Direct electron transfer involving free-solute ferrocene in fluid electrolyte on an oxocuprate (Bi(Pb) 2223) electrode in the superconducting state, J. Am. Chem. Soc., 114 (1992) 9702-9704.
[43] R.L. Birke, Q. Huang, T. Spataru, D.K. Gosser, Electroreduction of a series of alkylcobalamins: mechanism of stepwise reductive cleavage of the Co−C bond, J. Am. Chem. Soc., 128 (2006) 1922-1936.
[44] D.H. Evans, One-electron and two-electron transfers in electrochemistry and homogeneous solution reactions, Chem. Rev., 108 (2008) 2113-2144.
[45] F. Ammar, J.-M. Savéant, Thermodynamics of successive electron transfers internal and solvation enthalpy and entropy variations in a series of polynitro compounds., J. Electroanal. Chem., 47 (1973) 115-125.
[46] J. Edwin, W.E. Geiger, Structural changes coupled to two-electron-transfer reactions: oxidation mechanism of pseudo-triple-decker complexes of Co and Rh, J. Am. Chem. Soc., 112 (1990) 7104-7112.
[47] D.T. Pierce, W.E. Geiger, Electrochemical kinetic discrimination of the single-electron-transfer events of a two-electron-transfer reaction: cyclic voltammetry of the reduction of the bis(hexamethylbenzene)ruthenium dication, J. Am. Chem. Soc., 114 (1992) 6063-6073.
[48] K.M. Kadish, C.L. Yao, J.E. Anderson, P. Cocolios, Electrochemical and spectroelectrochemical studies of monomeric rhodium(III) porphyrins in nonaqueous media, Inorg. Chem., 24 (1985) 4515-4520.
[49] N. Fietkau, C.A. Paddon, F.L. Bhatti, T.J. Donohoe, R.G. Compton, Cryo-electrochemistry in tetrahydrofuran: The regioselective electrochemical reduction of a phenyl sulfone: Fast-scan cyclic voltammetry investigations, J. Electroanal. Chem., 593 (2006) 131-141.
[50] C.A. Paddon, F.L. Bhatti, T.J. Donohoe, R.G. Compton, Cryovoltammetrically probing functional group reductive cleavage: alkyl-sulfur versus aryl-sulfur bond cleavage in an alkyl naphthyl thioether under single electron-transfer is temperature switchable, Chem. Commun., (2006) 3402-3404.
[51] A. Thibon-Pourret, F. Gennarini, R. David, J.A. Isaac, I. Lopez, G. Gellon, F. Molton, L. Wojcik, C. Philouze, D. Flot, Y. Le Mest, M. Reglier, N. Le Poul, H. Jamet, C. Belle, Effect of monoelectronic oxidation of an unsymmetrical phenoxido-hydroxido bridged dicopper(II) complex, Inorg. Chem., 57 (2018) 12364-12375.
[52] N.J. Stone, D.A. Sweigart, A.M. Bond, Effects of temperature and supporting electrolyte on the electrochemical oxidation of (benzene)tricarbonylchromium and other .pi.-hydrocarbon complexes, Organometallics, 5 (1986) 2553-2555.
[53] W.J. Bowyer, D.H. Evans, Electron transfer reactions and associated conformational changes, J. Electroanal. Chem., 240 (1988) 227-237.
[54] T.J. Del Castillo, N.B. Thompson, J.C. Peters, A synthetic single-site Fe nitrogenase: high turnover, freeze-quench (57)Fe Mossbauer data, and a hydride resting state, J. Am. Chem. Soc., 138 (2016) 5341-5350.
[55] R.P. Van Duyne, C.N. Reilley, Low-temperature electrochemistry. III. Application to the study of radical ion decay mechanisms, Anal. Chem., 44 (1972) 158-169.
[56] A.M. Bond, D.A. Sweigart, Low temperature electrochemistry of metalloporphyrins in dichloromethane: characterization of transient species, Inorg. Chim. Acta, 123 (1986) 167-173.
[57] W.J. Bowyer, D.H. Evans, Electrochemical reduction of vicinal dinitro compounds, J. Org. Chem., 53 (1988) 5234-5239.
[58] E.F. Dalton, S. Ching, R.W. Murray, Cryoelectrochemical study of the cleavage of radical anions of diiron and diruthenium carbonyl dimers, Inorg. Chem., 30 (1991) 2642-2648.
[59] A. Evans, M.I. Montenegro, D. Pletcher, The mechanism for the cathodic reduction of sulphur in dimethylformamide: low temperature voltammetry, Electrochem. Commun., 3 (2001) 514-518.
[60] Y. Huang, C.C. Neto, K.A. Pevear, M.M. Banaszak Holl, D.A. Sweigart, Y.K. Chung, Ligand substitution at 19-electron organometallic centers. Electrocatalytic CO substitution reactions of (methylcyclopentadienyl)Mn(CO)2NO+ and (indenyl)Mn(CO)2NO+, Inorg. Chim. Acta, 226 (1994) 53-60.
[61] Y. Zhai, Z. Zhu, S. Zhou, C. Zhu, S. Dong, Recent advances in spectroelectrochemistry, Nanoscale, 10 (2018) 3089-3111.
[62] L. Blum, Mean spherical model for a mixture of charged spheres and hard dipoles, Chem. Phys. Lett., 26 (1974) 200-202.
[63] L. Blum, Solution of a model for the solvent-electrolyte interactions in the mean spherical approximation, J. Chem. Phys., 61 (1974) 2129-2133.
[64] S.A. Adelman, J.M. Deutch, Exact solution of the mean spherical model for strong electrolytes in polar solvents, J. Chem. Phys., 60 (1974) 3935-3949.
[65] W.R. Fawcett, M. Opallo, The Kinetics of heterogeneous electron transfer reaction in polar solvents, Angew. Chem. Int. Ed., 33 (1994) 2131-2143.
[66] B.S. Brunschchwig, J. Logan, M.D. Newton, N. Sutin, A semi-classical treatment of electron-exchange reactions. Application to the hexaaquoiron(II)-hexaaquoiron(III) system, J. Am. Chem. Soc., 102 (1980) 57985809.

[67] T. T. Gennett, D.F. Milner, M.J. Weaver, Role of solvent reorganization dynamics in electron-transfer processes. Theory-experiment comparisons for electrochemical and homogeneous electron exchange involving metallocene redox couples., J. Phys. Chem., 89 (1985) 2787-2794.

Appendices

Appendix A: Butler-Volmer model

Within the popular Butler-Volmer approach, both forward and backward activation free energies for a monoelectronic reduction process vary linearly with the driving force $-F(E-E^{0\prime})$ according to the values of $-\alpha$ and $(1-\alpha)$, respectively, as expressed in equations (A.1) and (A.2):

$$\Delta \boldsymbol{G}_{\mathrm{f}}^{\neq} = \Delta \boldsymbol{G}_{\boldsymbol{0}}^{\neq} + \boldsymbol{\alpha F}(\boldsymbol{E}-\boldsymbol{E}^{\boldsymbol{0\prime}}) \qquad \text{(A.1)}$$

$$\Delta G_{\mathrm{b}}^{\neq} = \Delta G_{0}^{\neq} + (\alpha-1)F(E-E^{0\prime}) \qquad \text{(A.2)}$$

where α is the transfer coefficient of the redox reaction.

The equations (A.1) and (A.2) indicate that a high driving force (i.e. $F(E^0-E) > 0$) merely favors the reduction process since $\Delta G_{\mathrm{f}}^{\neq}$ decreases proportionally to α, whereas $\Delta G_{\mathrm{b}}^{\neq}$ increases proportionally to $(\alpha-1)$ [26]:

According to the equations (A.1) and (A.2), both forward k_{f} and backward k_{b} rate constants can be written in Arrhenius form as shown by equation (A.3) and (A.4):

$$k_{\mathrm{f}} = k^0 \exp\left[-\frac{\alpha F}{RT}(E-E^{0\prime})\right] \qquad \text{(A.3)}$$

$$k_{\mathrm{b}} = k^0 \exp\left[\frac{(1-\alpha)F}{RT}(E-E^{0\prime})\right] \qquad \text{(A.4)}$$

Where k^0 is the standard rate constant.

From equations (A.3) and (A.4), the "current-overpotential equation" based on the Butler-Volmer assumption is given by the equation (A.5) :

$$i = i^0\left\{\frac{C_{\mathrm{O}}(0,t)}{C_{\mathrm{O}}^*}\exp\left[\frac{-\alpha F}{RT}\left(E-E_{\mathrm{eq}}\right)\right] - \frac{C_{\mathrm{R}}(0,t)}{C_{\mathrm{R}}^*}\exp\left[\frac{(1-\alpha)F}{RT}\left(E-E_{\mathrm{eq}}\right)\right]\right\} \qquad \text{(A.5)}$$

Where i^0 represents the exchange current as written in equation (A.6):

$$i_0 = FAk^0 C_{\mathrm{O}}^{*(1-\alpha)} C_{\mathrm{R}}^{*\alpha} \qquad \text{(A.6)}$$

[C_{O}^* and C_{R}^* are bulk concentrations in oxidized and reduced active species respectively, and E_{eq} is the equilibrium potential.]

When assuming no mass transfer effects (well-stirred solution, or surface concentrations which approach bulk concentrations), the "current-overpotential equation" (A.5) simplifies to the well-known "Butler-Volmer equation" (A.7):

$$i = i^0 \left\{ \exp\left[\frac{-\alpha F}{RT}\left(E - E_{\mathrm{eq}}\right)\right] - \exp\left[\frac{(1-\alpha)F}{RT}\left(E - E_{\mathrm{eq}}\right)\right]\right\} \qquad \text{(A.7)}$$

At low overpotential values, the equation (A.7) yields the expression of the charge transfer resistance R_{ct} :

$$R_{\mathrm{ct}} = \frac{RT}{Fi_0} \qquad \text{(A.8)}$$

The equation (A.8) is typically used for the determination of the standard rate constant values for sluggish systems as found at low temperature by emplying a.c. impedance measurement. This can be carried out by fixing the E_{dc} value equal (or close) to E_{eq} and by applying a potential amplitude E_{ac}which is sufficiently low to remain under activation control.

Appendix B: Marcus-Hush model

The classical treatment of electron transfer reactions considers the need for reorganization of the inner coordination shells (intramolecular configuration changes) of the reactants and the readjustment of the surrounding solvent dipoles prior to the electron transfer. Moreover, the electron transfer occurs at the intersection of the reactant and product free energy surfaces in a way that electronic levels are isoenergetic and nuclear motion can be neglected according to the Franck-Condon principle. When the donor and acceptor interact electronically, a quantum mechanical splitting occurs at the intersection between the reactant and product free energy surfaces, giving rise to two separate, upper and lower free energy surfaces (**Erreur ! Source du renvoi introuvable.**). The electron transfer may be adiabatic or non-adiabatic, depending on the degree of this splitting, which also affects (lowers) the activation free energy for the reaction. In the adiabatic case, the splitting is large enough that, on passage through the intersection region, the system stays on the lower free energy surface and the probability of passage from reactants to products is unity. In the non-adiabatic case, the splitting is not large enough to prevent there being some crossing from the lower to the upper free energy surface on passage through the intersection region and the probability of passage from reactants to products is thus less than unity. The resulting expressions for the Gibbs energies of activation associated with the forward and backward reactions for an heterogeneous electron transfer, $\Delta G_{\mathrm{f}}^{\neq}$, $\Delta G_{\mathrm{b}}^{\neq}$, are given in equations (12) and (13), assuming that (i) the reactant is centered at some fixed position with respect to the electrode, (ii) the standard free energies depend quadratically on the reaction coordinate, and (iii) the work terms that involve the energy changes produced in bringing charge reactants and products close to a charged electrode can be neglected in the presence of large excess of supporting salt.

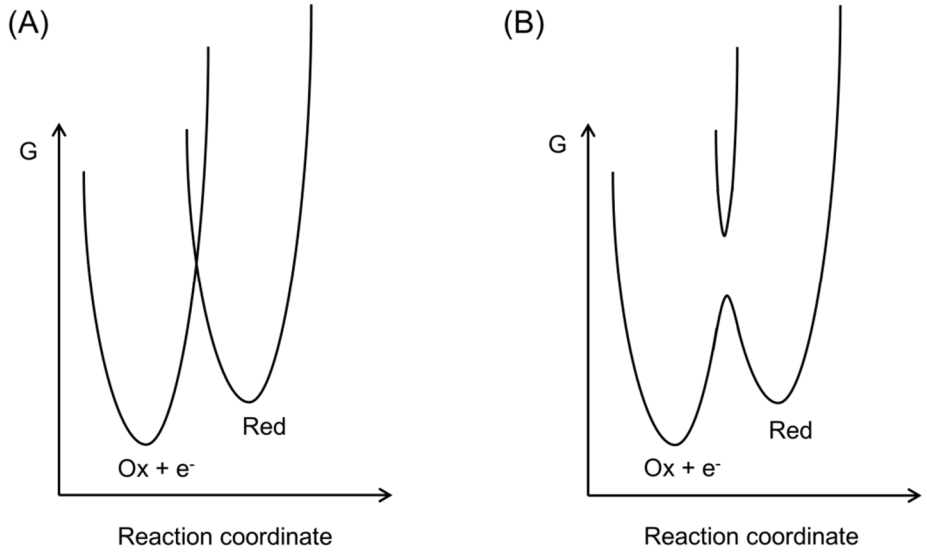

Figure B.13. Energy curves for the reduction reaction (Ox +e^- = Red); (A) without the splitting of the intersection caused by the electronic interaction between acceptor and donor, and (B) with the interaction. If the splitting is large enough, the system will stay on the lower surface and the reaction will be adiabatic. Insufficient splitting will allow the system to remain, on occasion, on the reactant surface after crossing of the intersection region, in which case the reaction will be non-adiabatic.

The reorganization energy is the sum of an inner component λ_i (intramolecular) being largely determined by the composition of the redox center, and an outer-sphere term λ_o which is function of the solvent dielectric. Assuming that the normal modes of the reactant remain harmonic over the range of distortion needed, the inner-sphere reorganization energy λ_i can be determined by summing over the normal vibrational modes of the reactant as shown in equation (B.1):

$$\boldsymbol{\lambda_i = \sum_j 0.5 f_j (\Delta q_j)^2} \qquad \text{(B.1)}$$

Where f_j is the force constant of the *j*th bond in the reactant, and Δq_j is the change in bond length in going from the reduced to the oxidized form.

The outer-sphere reorganization energy, λ_o is calculated by considering the solvent as a dielectric continuum, and the reactant as a sphere of radius a_r, leading to equation (B.2) for an electrode reaction:

$$\boldsymbol{\lambda_o = \frac{N_A e_0^2}{8\pi\varepsilon_0}\left(\frac{1}{a_r} - \frac{1}{R}\right)\left(\frac{1}{\varepsilon_{op}} - \frac{1}{\varepsilon_s}\right)} \qquad \text{(B.2)}$$

Where N_A is the Avogadro constant, e_0 is the fundamental electronic charge, ε_{op} and ε_s are the optical and static (zero frequency) dielectric constants, respectively, ε_0 is the permittivity of free space, and R is taken as the distance from the center of the molecule to the electrode. The value of R^{-1} is often neglected in the calculations in respect to a_r^{-1} considering the small size of the electroactive molecules.

A more sophisticated expression of λ_o has been proposed, namely the Mean Spherical Approximation (MSA) [62-64], which essentially accounts for polarizability, softness and non-sphericity of solvent molecules of radius a_{solv}, by inclusion of optical and static MSA polarization parameters (δ_{op} and δ_s) in the classical expression, hence leading to the equation (B.3):

$$\boldsymbol{\lambda_o = \frac{N_A e_0^2}{8\pi\varepsilon_0}\left[\left(1-\frac{1}{\varepsilon_{op}}\right)\frac{1}{(a_r+a_{solv}/\delta_{op})}-\left(1-\frac{1}{\varepsilon_s}\right)\frac{1}{(a_r+a_{solv}/\delta_s)}\right]} \qquad \text{(B.3)}$$

Values of δ_{op} and δ_s can be evaluated from the dielectric constants ε_{op} and ε_s according to equations (B.4) and (B.5):

$$\boldsymbol{16\varepsilon_{op} = \delta_{op}^{\ 2}(1+\delta_{op})^4} \qquad \text{(B.4)}$$

$$\boldsymbol{16\varepsilon_s = \delta_s^{\ 2}(1+\delta_s)^4} \qquad \text{(B.5)}$$

For polar solvents, the static polarization parameter δ_s is in the range 2.0 to 2.9, whereas δ_{op} is close to unity. Nevertheless, the validity of the equation (B.3) was questioned [65]. The optical MSA polarization parameter δ_{op} was proposed to be neglected in the equation (B.3) and δ_s to be evaluated from the Gibbs solvation energies of simple monoatomic, monovalent ions. According to this approximation, calculations yield a reorganization energy value which is significantly lower than the experimental results.

Within the Marcus theory, the pre-exponential term A' of the Arrhenius-like equation has been considered for adiabatic and non-adiabatic cases [24]:

$$\boldsymbol{A' = K_P\nu_n\kappa_{el} = Z_{el}\kappa_{el}} \qquad \text{(B.6)}$$

Hence leading to the general equation (B.7) for the standard rate constant:

$$\boldsymbol{k^0 = K_P\nu_n\kappa_{el}\exp\left(\frac{-\Delta G_0^{\ddagger}}{RT}\right)} \qquad \text{(B.7)}$$

where K_P is a precursor equilibrium constant, representing the ratio of the reactant concentration in the reactive position at the electrode (the precursor state) to the concentration in bulk solution; ν_n is the nuclear frequency factor (s^{-1}), which represents the frequency of attempts on the energy barrier (generally associated with bond vibrations and solvent motion), κ_{el} is the electronic transmission coefficient (related to the probability of electron tunneling) and Z_{el} the gas-phase collision number.

For an adiabatic reaction, $\kappa_{el} = 1$, then A' simplifies to $Z_{el} = K_P\nu_n$. This situation occurs when the reactant is considered to be close to the electrode, such that there is strong coupling between the reactant and the electrode. Z_{el} can be estimated by assuming solvent and electroactive species as hard spheres of molecular mass M (see equation (B.8)):

$$Z_{el} = \left(\frac{k_B T}{2\pi M}\right)^{1/2} \quad \text{(B.8)}$$

For a non-adiabatic electron transfer, the electronic transmission coefficient κ_{el} is below unity. Treatment by a quantum mechanical approach gives an approximated value for κ_{el} that is a function of the reorganization energy and temperature (equation (B.9)), assuming a small value for the electronic coupling energy H [66]:

$$\kappa_{el} = \frac{2\pi^{3/2} H^2}{\lambda^{1/2}} \left(\frac{F}{RT}\right)^{3/2} \quad \text{(B.9)}$$

Alternatively, the pre-exponential factor A' can be determined from K_P and ν_n. The nuclear frequency factor ν_n is given by equation (B.10) by considering solvent dynamics in the vicinity of the barrier top, through the contributions from bond vibrations (inner-shell) and solvent reorientation (outer-shell):

$$\nu_n = \left(\frac{\nu_o^2 \lambda_o + \nu_i^2 \lambda_i}{\lambda_o + \lambda_i}\right)^{1/2} \quad \text{(B.10)}$$

where ν_o and ν_i are the characteristic frequencies associated, respectively, with the inner-shell and outer-shell components.

The value of the inner-shell component ν_i can be estimated from Raman spectroscopic data (for example, ν_i = 6 ps^{-1} for decamethylferrocene in polar solvents) [67]. The outer shell component ν_o can be evaluated by using the solvent dynamics approach which considers that the outer-shell nuclear frequency term is principally dependent on solvent repolarization during the electron transfer. The outer-shell frequency is generally expressed as in equation (29), where τ_L is the longitudinal solvent relaxation time for the solvent:

$$\nu_o = \left(\frac{1}{4\tau_L}\right)\left(\frac{\lambda_o}{\pi RT}\right)^{1/2} \quad \text{(B.11)}$$

τ_L is an indicator of the friction between solvent molecules. Hence, it increases when concerted motions of the surrounding solvent are impeded, causing unfruitful crossings of the transition barrier. In a general manner, this situation occurs when τ_L > 1 ps, such as when the viscosity of the medium is raised by working at low temperatures. For solvents with a Debye dynamical behavior (i.e. their dielectric loss spectra can be described in terms of a single relaxation time τ_D), the expression for τ_L is:

$$\tau_L = (\varepsilon_\infty / \varepsilon_s)\tau_D \quad \text{(B.12)}$$

With

$$\tau_D = \frac{2r^3}{3Da} \quad \text{(B.13)}$$

where ε_∞ is the high-frequency dielectric constant determined in the far infrared, ε_s is the static (zero frequency) dielectric constant, τ_D is the Debye relaxation time, D and a are, respectively, the diffusion coefficient and hydrodynamic radius of the electroactive species and r the radius of the solvent molecule.

By combining equations (B.11-B.13), ν_o can be expressed as following:

$$\boldsymbol{\nu_o} = \left(\frac{3Da}{8r^3}\right)\left(\frac{\varepsilon_s}{\varepsilon_\infty}\right)\left(\frac{\lambda_o}{\pi RT}\right)^{1/2} \qquad \text{(B.14)}$$

Appendix C: Marcus-Density of States (DOS) model

In the frame of the Marcus-DOS model, the activation energies, $\Delta G_f^{\neq}(\varepsilon)$ and $\Delta G_b^{\neq}(\varepsilon)$, for the transfer to states of energy ε are given by the equation (C.1) and (C.2) derived from equations (12) and (13):

$$\boldsymbol{\Delta G_f^{\neq}(\varepsilon)} = \frac{[\lambda-\varepsilon+F(E-E^0)]^2}{4\lambda} \qquad \text{(C.1)}$$

$$\boldsymbol{\Delta G_b^{\neq}(\varepsilon)} = \frac{[\lambda+\varepsilon-F(E-E^0)]^2}{4\lambda} \qquad \text{(C.2)}$$